For Reference

NOT TO BE TAKEN FROM THIS ROOM

THE UNIVERSITY OF ALBERTA

SEARCH FOR A 5.6 MEV LEVEL IN Li^7

by

ARIE REEDYK

A THESIS

SUBMITTED TO THE FACULTY OF GRADUATE STUDIES

IN PARTIAL FULFILMENT OF THE REQUIREMENTS FOR THE DEGREE

OF MASTER OF SCIENCE

DEPARTMENT OF PHYSICS

EDMONTON, ALBERTA

OCTOBER, 1963

UNIVERSITY OF ALBERTA

FACULTY OF GRADUATE STUDIES

The undersigned certify that they have read, and re-
commend to the Faculty of Graduate Studies for acceptance, a
thesis entitled, "Search for a 5.6 Mev Level In Li^7", submitted
by Arie Reedyk in partial fulfilment of the requirements for
the degree of Master of Science.

ABSTRACT

A review of the Rotational Model of a nucleus is given.
The application of this model to Li^7 is shown to lead to the
prediction of a level at 5.6 Mev excitation in that nucleus.
An experimental search has been made for this predicted level
by observation of the charged reaction products resulting from
deuteron bombardment of Li^6. No proton group corresponding to
a Li^7 level in the vicinity of 5.6 Mev excitation has been
observed. From the charged particle spectra resulting
from 1.90 Mev bombarding deuterons, an upper limit of
.05 mb/sterad is assigned to the backward angle differential
cross-section for the $Li^6(d,p)Li^7$ reaction going to any
possible narrow level around 5.6 Mev excitation in Li^7.

ACKNOWLEDGEMENTS

TABLE OF CONTENTS

LIST OF FIGURES

I   INTRODUCTION

     The prediction of a level scheme is a severe test of a

nuclear model's applicability. In this thesis the applica-

bility of the strong coupling rotational model to the Li^7

nucleus is studied. In particular, an attempt is made to

locate experimentally a nonobserved low lying energy level

in Li^7 which is predicted as a result of the application of

the strong coupling rotational model to this nucleus.

     Chapter II of this thesis is devoted to the details of

the strong coupling rotational model and its application to

Li^7. The level scheme predicted by this model is compared to

the experimental energy scheme. The overall agreement is

found to be surprisingly good except for one serious discre-

pancy. On the basis of the rotational model, a level is

predicted at 5.6 Mev excitation of Li^7. Such a level has not

been observed experimentally.

     A number of nuclear reaction experiments are possible

that would allow a search for such a level. It was decided

to use the $Li^6(d,p)Li^7$ reaction and to look for proton groups

at backward angles. Chapter III is devoted to a discussion

of the (d,p) reaction and a survey of past work on the $Li^6(d,p)Li^7$

reaction.

     The fourth and final chapter relates details of the

experiment performed. The main difference between the experi-

mental technique used here and that used in the past lies in the

means of detecting the charged particle spectra. In the present

experiment a solid state detector is used. The resolution

of this detector is better than 1% and the allowable count

rate is high. Since good statistical results can thus be

readily obtained, it was hoped that either a proton group

from the reaction in question would be observed or a low

upper limit could be placed on the reaction cross-section.

II. THE STRONG COUPLING ROTATIONAL MODEL APPLIED TO Li[7]

1. Introduction

It has been found that the energy spectra of certain nuclei display strikingly simple features that can be explained in terms of a separation between nucleonic motion relative to a nucleus fixed coordinate system and collective motion of the nucleus as a whole in space. There are two types of collective motion, vibrational and rotational.

The spectra associated with vibrational motion of the nucleus occur for nuclei that have a spherical equilibrium shape. In that case the energy levels are considered to be due to the nucleus' ability to perform small oscillations about the spherical equilibrium shape. One is able to describe these oscillations in terms of a set of normal modes. For small amplitudes these modes of oscillation are independent and each is equivalent to a harmonic oscillator.

However, not all nuclei have a spherical equilibrium shape. If a nucleus has particles in unfilled shells, these particles will tend to distort the nuclear shape so as to adjust it to their own density distribution. The more nucleons there are in unfilled shells the greater will be the tendency towards deformation. At the same time, there is at work an opposing tendency trying to retain the spherical shape. This is the effect of the pairing forces which tend to couple pairs of equivalent nucleons to a state of zero angular momentum, that is, a spherically symmetric state. Finally, for sufficiently

many particles outside closed shells, the spherical shape
becomes unstable and changes to an ellipsoidal equilibrium
shape. This ellipsoidal equilibrium shape is constant in
time but generally rotates in space.

It is sometimes possible to separate between this
collective motion of the nucleus and the intrinsic motion
of the nucleons relative to a coordinate system fixed in the
ellipsoid. This corresponds to the assumption that the
nuclear state may be described by a wave function of the form
$\Psi = \chi \cdot \phi_{vib} \cdot \xi_{rot}$. Here χ represents the intrinsic motion of
the individual nucleons in the field resulting from the ellip-
soidal equilibrium shape of the nucleus. The factor ϕ_{vib}
describes the vibrations of the nucleus around its equilibrium
shape. The last factor, ξ_{rot}, represents the collective
rotational motion of the nucleus. For appreciably deformed
nuclei, it is found that the energy difference between successive
vibrational levels is much greater than between successive rota-
tional levels. Therefore, if one is dealing with a nucleus
that is not too near a closed shell configuration, the nucleus
will for the lower levels be in the vibrational ground state. If
this is the case, the rotational model of the nucleus is said to
apply. This section will be devoted to a closer examination of
this rotational model and how it may be applied to Li[7].

2. Intrinsic Motion

For quantitative predictions of the intrinsic motion variables,

use can be made of the tabulated results in a paper by S. G.

Nilsson (Ni55) titled "Binding States of Individual Nucleons

in Strongly Deformed Nuclei". In this paper the effect on the

individual nuclear nucleon of all other nucleons is approximated

by the following Hamiltonian.

$$H = H_0 + C \vec{l} \cdot \vec{s} + D \vec{l}^2, \tag{II-1}$$

where $H_0 = -\frac{\hbar^2}{2M} \Delta' + \frac{M}{2} (\omega_x^2 x'^2 + \omega_y^2 y'^2 + \omega_z^2 z'^2),$ $\tag{II-2}$

where x',y', and z' are the coordinates of a particle in a

coordinate system that permanently coincides with the nucleus'

principal axes. This is similar to the approach taken in the

usual shell model calculations except that now the potential

is not spherically symmetric as ω_x, ω_y and ω_z are not necessarily

all equal. The $\vec{l}^2$ term is inserted to depress high angular

momentum states. The overall Hamiltonian is in that way some-

where intermediate between the oscillator and square well

potential, as it should be. For the spherically symmetric case

the Hamiltonian eigenvalues must have the known sequence of

single particle levels considered in the shell mode. This puts

stringent restrictions on the choice of C and D. Nilsson restricts

himself to cylindrical symmetry and introduces a deformation para-

meter δ defined by the following equations.

$$\omega_x^2 = \omega_y^2 = \omega_0^2 \left(1 + \frac{2}{3} \delta\right) \tag{II-3}$$

$$\omega_z^2 = \omega_0^2 \left(1 - \frac{4}{3} \delta\right)$$

If the $\vec{l} \cdot \vec{s}$ and $\vec{l}^2$ terms are neglected the problem is separable

in x', y', and z'. In that case a change in any of ω_x, ω_y, or ω_z, only produces a change in the scale of the wave function along the corresponding axis. For example, the scale along the x' axis is proportional to $1/\sqrt{\omega_x}$. Then, since nuclear volume is considered incompressible, the following relation applies.

$$\omega_x \omega_y \omega_z = \text{constant}. \tag{II-4}$$

For the cylindrical symmetry assumed it then follows that

$$\omega_o(\delta) = \mathring{\omega}_o \left(1 - \frac{4}{3}\delta^2 - \frac{16}{27}\delta^3\right)^{-\frac{1}{6}}, \tag{II-5}$$

where $\mathring{\omega}_o$ is the value of $\omega_o(\delta)$ for $\delta = 0$.

Introduction of $\quad x = \sqrt{\frac{M\omega_o}{\hbar}}\, x'$, $\quad y = \sqrt{\frac{M\omega_o}{\hbar}}\, y'$,

and $\quad z = \sqrt{\frac{M\omega_o}{\hbar}}\, z'$ \tag{II-6}

and regrouping gives $\quad H_o = \mathring{H}_o + H_\delta$, \tag{II-7}

where $\mathring{H}_o = \hbar\omega_o \frac{1}{2}\left[-\Delta + r^2\right]$, \tag{II-8}

and $\quad H_\delta = -\delta\hbar\omega_o \frac{4}{3}\sqrt{\frac{\pi}{5}}\, r^2 Y_{20}$. \tag{II-9}

To solve for the eigenstates of the single particle Hamiltonian, H, a representation is chosen with $\mathring{H}_o$, $\vec{\ell}^2$, $\vec{\ell}_z$, and S_z diagonal. It is noted that the latter three commute with the first. Their quantum numbers are denoted by ℓ, Λ, and Σ respectively. It is further noted that none of $\vec{\ell}^2$, ℓ_z, and S_z commute with the Hamiltonian H_o. However, $j_z = \ell_z + S_z$ is an operator commuting with H_o. The quantum number corresponding to j_z is denoted by Ω. The base vectors of this representation are denoted by $|N\ell\Lambda\Sigma\rangle$, where $\Lambda + \Sigma = \Omega$, and N is the total number of

oscillator quanta so that

$$\overset{\circ}{H_o}\,|N\ell\,\Lambda\Sigma\rangle = \left(N+\tfrac{3}{2}\right)\hbar\omega_o\,|N\ell\,\Lambda\Sigma\rangle \qquad (\text{II-10})$$

In the representation chosen $\vec{\ell}^{\,2}$ and $\overset{\circ}{H_o}$ are diagonal. The non vanishing elements of $\vec{\ell}\cdot\vec{s}$ are

$$\langle N\ell\,(\Lambda\pm1)\mp\tfrac{1}{2}|\vec{\ell}\cdot\vec{s}|N\ell\,\Lambda\pm\tfrac{1}{2}\rangle = \tfrac{1}{2}\sqrt{(\ell\mp\Lambda)(\ell\pm\Lambda+1)} \qquad (\text{II-11})$$

and $\langle N\ell\,\Lambda\pm\tfrac{1}{2}|\vec{\ell}\cdot\vec{s}|N\ell\,\Lambda\pm\tfrac{1}{2}\rangle = \pm\tfrac{1}{2}\Lambda.$

The selection rules for non vanishing matrix elements of $r^2 Y_{20}$ in the chosen representation are

$$\Lambda = \Lambda' \qquad \Sigma = \Sigma' \qquad \ell = \begin{cases}\ell'\\\ell'\pm2\end{cases} \qquad N = \begin{cases}N'\\N\pm2\end{cases}. \qquad (\text{II-12})$$

This indicates a coupling between states whose oscillator quantum numbers differ by 2. Nilsson reasons that since the energy difference between different N shells is much larger than the corresponding non-diagonal coupling energies, the latter may be neglected to a good degree of approximation. Hence N and Ω are both considered to be good quantum numbers of the system in question.

For convenience Nilsson introduces the following dimensionless parameters. Parameters μ and χ are introduced to take the place of C and D in the following manner.

$$\chi = -\tfrac{1}{2}\frac{C}{\hbar\omega_o} \qquad (\text{II-13})$$

$$\mu = \frac{2D}{C} \qquad (\text{II-14})$$

A χ-dependent deformation parameter, η, is introduced.

$$\eta = \frac{\delta}{\chi} \frac{\omega_0(\delta)}{\omega_0} = \frac{\delta}{\chi} \left[1 - \frac{4}{3} \delta^2 - \frac{16}{27} \delta^3 \right]^{-\frac{1}{6}}. \tag{II-15}$$

Setting $\quad U = -\frac{4}{3} \sqrt{\frac{\pi}{5}} \, r^2 \, Y_{20} \tag{II-16}$

allows H_δ to be written as

$$H_\delta = \delta \hbar \omega_0 \, U = \chi \hbar \dot{\omega}_0 \, \eta \, U. \tag{II-17}$$

Introduction of the above parameters allows the single particle

Hamiltonian to be written as

$$H = \mathring{H}_0 + \chi \hbar \dot{\omega}_0 \, R, \tag{II-18}$$

where $R = \eta U - 2 \vec{\ell} \cdot \vec{s} - \mu \vec{\ell}^2. \tag{II-19}$

The dimensionless operator R depends on only two parameters,

η and μ. The diagonalization of R was carried out by computer

for various values of η and the corresponding eigenvalues,

$r_\alpha^{N\Omega}(\eta)$, are tabulated in Nilsson's paper. The energy eigen-

values of the total individual particle Hamiltonian are then

given by

$$E_\alpha^{N\Omega} = \left(N_\alpha + \frac{3}{2} \right) \hbar \, \omega_0(\delta) + \chi \hbar \mathring{\omega}_0 \, r_\alpha^{N\Omega}. \tag{II-20}$$

The corresponding eigenvector is represented by $|N\Omega\alpha\rangle$, where

α is a label on the different eigenvalues of the R matrix.

As for the choice of μ and χ; This must be such that for $\delta = 0$

the sequence of levels of the shell model is reproduced. The

values of μ and χ can be chosen different for different N

values. Nilsson makes the following choices for μ.

$\mu = 0 \quad$ for N = 0, 1, 2 $\qquad \mu = 0.45$ for N = 4, 5, 6

$\mu = 0.35$ for N = 3 $\qquad\qquad \mu = 0.40$ for N = 7

These choices of μ mean that for the lower N values a pure
oscillator potential is used and for the higher N values the
potential is varied towards a square well. Nilsson takes a
value of 0.05 for χ for all levels. Later workers (Li58)
found it necessary to use slightly higher values to fit empe-
rical data on various nuclei. Nilsson obtains a reasonable
value for ω_0 by taking the mean value of r^2 for all the
nucleons to be equal to $\frac{3}{5}(1.2 \times 10^{-13} A^{1/3})^2$ cm^2. This corresponds
to a value of $\hbar\omega_0^{\circ}$ of 41 $A^{-1/3}$ Mev.

The tables in which Nilsson presents the computed results
give the following information. All possible eigenstates up
to and including N = 6 are listed. For each value of N, Ω
can have half integer values ranging from 1/2 to N + 1/2,
that is, there are N + 1 possible values for Ω corresponding
to a certain N value. The tables display for each combination
of N and Ω the eigenvalues $r_\alpha^{N\Omega}(\eta)$ for seven evenly spaced
values of η from -6 to 6. For each $r_\alpha^{N\Omega}(\eta)$ the corresponding
eigenvector is given as the coefficients in a linear combi-
nation of $|N\ell(\Omega+\frac{1}{2})-\frac{1}{2}\rangle$ and $|N\ell(\Omega-\frac{1}{2})+\frac{1}{2}\rangle$ for all allowable ℓ
values.

From the above mentioned tables it is possible to deter-
mine the total intrinsic energy of a nucleus and its equili-
brium deformation. If only two body forces are assumed the
Hamiltonian for the ith particle is given by

$$H_i = T_i + V_i = T_i + \sum_{j \, j \neq i} V_{ij} \tag{II-21}$$

Therefore the Hamiltonian for the whole nucleus is

$$H_{int} = \sum_i T_i + \tfrac{1}{2} \sum_{ij\,(i \neq j)} V_{ij}$$

$$= \tfrac{1}{2} \sum_i H_i + \tfrac{1}{2} \sum_i T_i \qquad\qquad (II\text{-}22)$$

$$= \tfrac{3}{4} \sum_i H_i - \tfrac{1}{4} \sum_i (V_i - T_i)$$

Nilsson shows that $\quad \langle V_i - T_i \rangle = \langle U_i \rangle$, $\qquad\qquad$ (II-23)

where $\quad U_i = C\,\vec{\ell}\cdot\vec{s} + D\vec{\ell}^{\,2}$ $\qquad\qquad\qquad\qquad$ (II-24)

If U_i is put in units of $\tfrac{3}{4}\hbar\overset{\circ}{\omega}_o$, the total energy eigenvalues of the total intrinsic Hamiltonian are given by

$$E_{int} = \tfrac{3}{4}\hbar\overset{\circ}{\omega}_o \left[\sum_i (N_i + \tfrac{3}{2})\left(1 - \tfrac{1}{3}\varepsilon^2 - \tfrac{2}{27}\varepsilon^3\right)^{-\tfrac{1}{3}} \right. \qquad (II\text{-}25)$$
$$\left. + \sum_i \mathcal{X}r_i^{N\Omega} - \tfrac{1}{4}\sum_i \langle U_i \rangle \right]$$

where ε is another deformation parameter readily connected to δ by considering its defining equations,

$$\omega_x = \omega_y = \omega_o(\varepsilon)\left(1 + \tfrac{1}{3}\varepsilon\right) \qquad\qquad (II\text{-}26)$$

$$\omega_z = \omega_o(\varepsilon)\left(1 - \tfrac{2}{3}\varepsilon\right) \qquad\qquad (II\text{-}27)$$

To find the total intrinsic nuclear energy, E_{int}, corresponding to a certain combination of individual particle levels, E_{int} is evaluated as a function of the deformation parameter δ , and the minimum value that E_{int} takes is the proper value. The value of δ at which E_{int} is a minimum gives the deformation of that particular intrinsic state. The lowest E_{int} encountered by considering all possible particle level combinations gives the ground state. Other minima represent excited nuclear levels. The total intrinsic wave function of all the nucleons is the product of the appropriately symme-

trized wave functions of each occupied particle state.

A glance at Nilsson's tables reveals that for any parti-
cular particle state defined by N and Ω the base vectors in
terms of which the eigenvectors are given have either all odd
or all even ℓ. The parity of the state is positive for even
ℓ and negative for odd ℓ.

The Ω_p of the individual nucleons add up to a total
component of intrinsic angular momentum along the nuclear
symmetry axis. The ground state of a nucleus is obtained by
filling the particle states pair wise with particles of
opposite Ω_p. As a result, for an even even nucleus in the
ground state $\Omega = 0$ and for an odd A nucleus in the ground state
the total Ω is equal to Ω_p of the last odd particle. In odd
odd nuclei the last odd neutron and proton each contribute
some Ω_p and the total is either their sum or difference.

3. Rotational Motion

As pointed out above, the Ω_p of all the nuclear particles
add up to some total Ω. In particular, in the case of an odd
A nucleus the total Ω is equal to the Ω_p of the last odd parti-
cle. As a model of a nucleus of this type Kerman (Ke55) takes
the system of a single particle coupled to a rigid top by a
potential $V(\vec{r})$. The Hamiltonian for this system is

$$H = \frac{p^2}{2m} + V(\vec{r}) + \sum_{k=1}^{3} \frac{\hbar^2}{2J_k}(I_k - j_k)^2$$

(II-28)

where $\vec{p}$, $\vec{J}$, and $\vec{r}$ are respectively the linear momentum, angu-
lar momentum, and position vector of the particle in the

coordinate system whose axes correspond to the instantaneous
position of the principal axes of the top. The vector $\vec{I}$
is the total angular momentum of the system and m is the
reduced mass of the system. In analogy to the actual shape of
deformed nuclei it is useful to consider that both the top and
the potential V(r) display axial symmetry. In that case
$\mathfrak{I}_1 = \mathfrak{I}_2 = \mathfrak{I}$. Rewriting (II-28) in a more useful form gives

$$H = H_0 + \frac{\hbar^2}{2\mathfrak{I}_3}(I_3 - j_3)^2 + \frac{\hbar^2}{2\mathfrak{I}}(I^2 - I_3^2 - j_3^2) + RPC \, , \qquad (II-29)$$

where $H_0 = \frac{p^2}{2m} + V(\vec{r}) + \frac{\hbar^2}{2\mathfrak{I}} j^2$ (II-30)

and $RPC = -\frac{\hbar^2}{2\mathfrak{I}}(I_+ j_- + I_- j_+)$, (II-31)

where $I_\pm = I_1 \pm i I_2$ and $j_\pm = j_1 \pm i j_2$. (II-32)

The term RPC defined above is an effect of the Coriolis force
on the particle and is short for the phrase "rotation particle
coupling". If the term RPC in the Hamiltonian may be neglected
then both I_3 and j_3 will commute with the Hamiltonian and
consequently will be good quantum numbers. Conventionally they
are designated by K and Ω respectively. H_o can in principal
be solved for the particle motion with Ω as one of the quantum
numbers as was outlined for a particular V($\vec{r}$) in the previous
sub-section. The energy spectrum corresponding to the Hamil-
tonian of equation (II-29) is then given by

$$E = E_\Omega^{(0)} + \frac{\hbar^2}{2\mathfrak{I}_3}(K - \Omega)^2 + \frac{\hbar^2}{2\mathfrak{I}}(I(I+1) - K^2 - \Omega^2) \qquad (II-33)$$

Kerman notes that all available data on rotational spectra in
nuclei indicates that only states for which K $=\Omega$ occur in the

regions of low excitation indicating that J_3 approaches zero,
Therefore, the spectrum of equation (II-33) reduces to

$$E = E_K^{(0)} + \frac{\hbar^2}{2J}\left(I(I+1) - 2K^2\right) \tag{II-34}$$

If the particle is strongly coupled to the rotator the
RPC is a small perturbation and the simple spectrum of equa-
tion (II-34) is evident. Even for strong coupling there is
one important deviation from this spectrum. This occurs for
the case where $K = \Omega = \frac{1}{2}$. In this case RPC has a diagonal matrix
element. Kerman (Ke59) shows that its contribution to the
energy is given by $a(-1)^{I+\frac{1}{2}}\left(I+\frac{1}{2}\right)$,

where $a = -\sum_J |c_j|^2 (-1)^{j+\frac{1}{2}} \left(j+\frac{1}{2}\right)$, $\tag{II-35}$

where the c_j are the normalized expansion coefficients of the
intrinsic wave functions in terms of eigenstates of the particle
angular momentum, $\vec{j} = \vec{l} + \vec{s}$. The parameter a is referred to as
the decoupling parameter as it corresponds to a partial decoup-
ling of the particle motion from the rotator. An expression
for the energy covering all possible cases of Ω is therefore
given by

$$E = E_K^{(0)} + \frac{\hbar^2}{2J}\left[I(I+1) - 2K^2 + \delta_{K,\frac{1}{2}}\, a(-1)^{I+\frac{1}{2}}\left(I+\frac{1}{2}\right)\right] \tag{II-36}$$

At the start of this sub-section the model assumed was
taken to be the model of an odd A nucleus in the ground state
with the single particle coupled to the top representing the
last odd nucleon in the nucleus. However the model can apply
just as well to any other nucleus in any state with the Ω
of the particle in the model now representing the total Ω of

all the nucleons.

If account is also taken of the vibrational motion of the nucleus, there will be a rotation-vibration term introduced in the energy. For a nucleus in the vibrational ground state this energy, $E_{vib-rot}$, is given by

$$E_{vib-rot} = B\left[I(I+1) + \delta_{k,\frac{1}{2}}\, a(-1)^{I+\frac{1}{2}}\left(I+\tfrac{1}{2}\right)\right]^2 \qquad (II-37)$$

where B gives a measure of the strength of the rotation-vibration interaction. The value of B is usually relatively small and in that case this term may for practical purposes be neglected.

The reflection symmetry of the nucleus implies that the collective motion part of the total nuclear wave function has even parity. The overall parity of the nuclear state is therefore determined by the intrinsic particle structure.

4. Application to Li^7

The theory outlined in the preceeding two sub-sections has been applied to Li^7 by Chesterfield & Spicer (Ch63).

Chesterfield and Spicer evaluated the total intrinsic energy of Li^7, E_{int}, as a function of the deformation parameter ϵ for various configurations. Use was made of Nilsson's tables for the appropriate $\eta_i^{N\Omega}$. Their results are displayed in figure II-1. The notation used to describe a configuration is the following. The main line numbers refer to the Nilsson particle level occupied and the associated superscripts are the number of nucleons at that level. The energy scale

DEFORMATION DEPENDENCE OF Li^7 INTRINSIC ENERGIES

FOR VARIOUS NUCLEAR CONFIGURATIONS
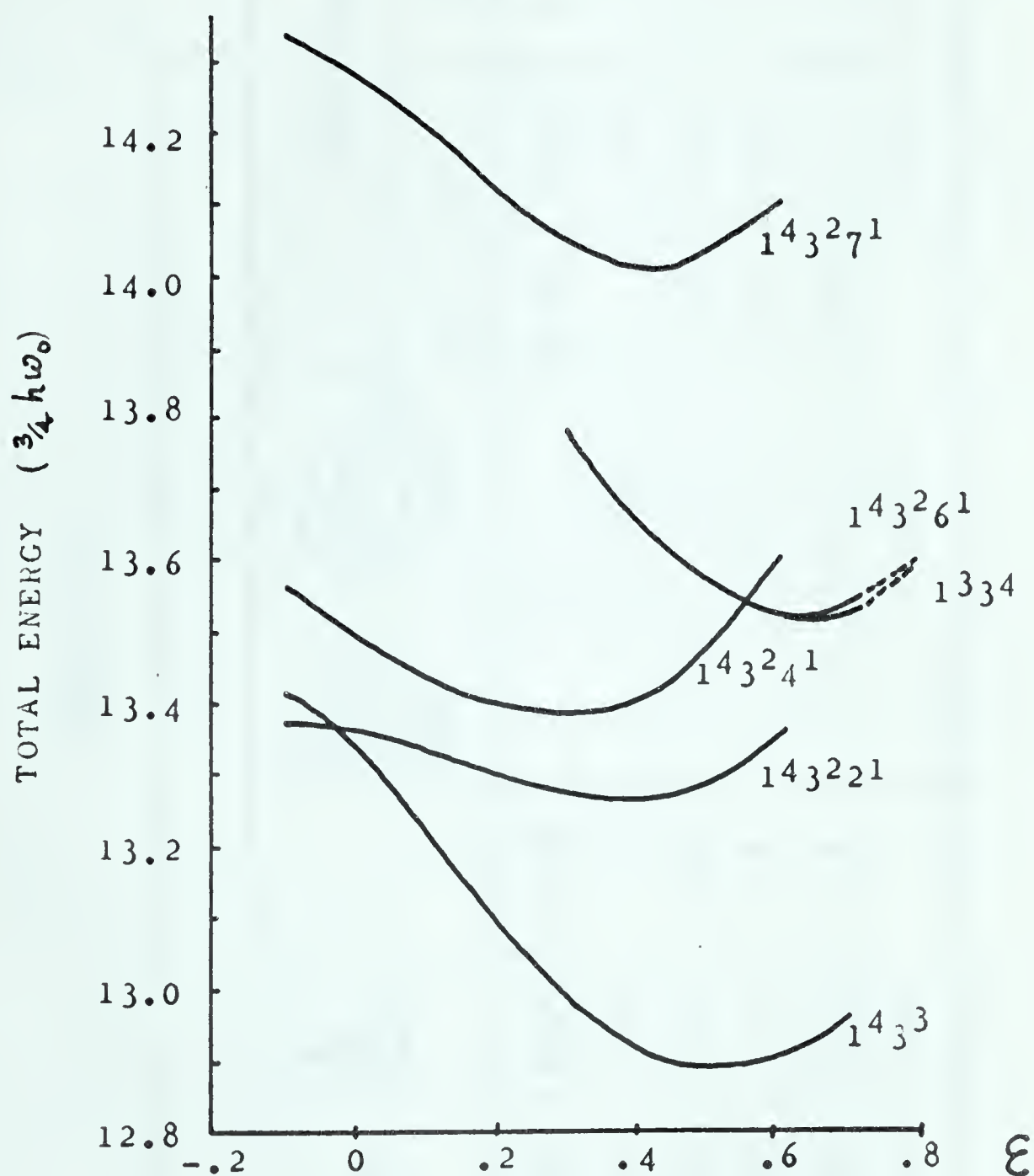
FIGURE II-1

TABLE II-1

DETAILS AND RESULTS OF ENERGY LEVEL CALCULATION FOR Li^7

Configuration	I^π	ε_{eq}	$\dfrac{\hbar^2}{2J}$ (MeV)	a	Pairing Energy contribution (MeV)	Energy without zero point correction (MeV)	Rotational Series			
							1/2	3/2	5/2	7/2
$1^4 3^3$	1/2$^-$	0.50	0.54	-1.36			0.48	-0.11	6.27	4.91
$1^4 3^2 2^1$	3/2$^-$	0.40	0.38			5.90		5.62	7.52	9.80
$1^4 3^2 4^1$	1/2$^-$	0.32	0.6	0.63		7.90	7.67	10.60	11.71	18.56
$1^4 3^2 6^1$	1/2$^+$	0.63	0.47	1.9		10.21	9.43	13.53	11.40	20.95
$1^3 3^4$	1/2$^+$	0.63	0.55	1.0	2.56	10.13	12.27	15.57	15.57	23.27
$1^4 3^2 7^1$	3/2$^+$	0.43	0.54			18.33		17.95	20.65	24.43

factor, $\hbar\omega_o$, was chosen to give the best overall fit to the
Li^7 level scheme. The value used was 22.4 Mev as compared
to a value of 21.5 Mev obtained from $41A^{-\frac{1}{3}}$. They also
found that setting $\chi = 0.08$ gave the best agreement with ob-
served levels. The results of their calculations are summa-
rized in a table, reproduced here as table II-1.

In table II-1, only single-particle excitations are
considered. The reason cited for omitting many-particle
excitations is that they would be more difficult to form
than single particle excitations.

Equation (II-36) gives an expression for the total
energy of a nucleus. It is common practice, however, not
to speak of the total energy of a nucleus but rather of
the excitation energy of a nucleus relative to its ground
state. This is equivalent to arbitrarily setting the
energy of the ground state equal to zero. This just intro-
duces an additive negative constant on the right hand side
of equation (II-36).

Another correction is necessary to equation (II-36).
In its development, a Hamiltonian was used that did not
exhibit the effect of nuclear pairing forces. However, as
long as no pairs are made or broken in going from one con-
figuration to another no correction is necessary. Difficulty
arises when a pair is made or broken. Chesterfield and Spicer
handle this problem in going from the $1^4 3^3$ configuration to
the $1^3 3^4$ configuration of Li^7 in a plausible but non-rigorous

manner. They reason that the pairing energy difference
between a Nilsson level 1 (s shell) and level 3 (p shell)
can be obtained from the difference in energies between the
$He^4(\gamma,p)$ and $Be^8(\gamma,p)$ thresholds. This corresponds to 2.56
Mev.

Each intrinsic configuration in the table gives rise
to a rotational series with spin I = K, K + 1, K + 2,........
The state for which I = K is referred to as the base state
of a series.

Chesterfield and Spicer found that the RPC and rota-
tion-vibration interaction terms were in effect small for
Li^7 and consequently neglected them in their calculations.
The $\frac{\hbar^2}{2J}$ for the various configurations were picked for best
agreement with experiment. The α were obtained from the
coefficients of the intrinsic eigenfunction expansions
given in Nilsson's tables. The rotational bands predicted
are compared to the experimentally observed levels in
figure II-2.

The four lowest experimental levels are all predicted
to be members of the rotational band based on the 0.478
Mev (1/2⁻) state, having spins of 3/2⁻, 1/2⁻, 7/2⁻, and
5/2⁻ respectively. With that interpretation the 7.47 Mev
(5/2⁻) observed state must belong to another rotational
band. If the 7.47 Mev state is considered a member of a
rotational series based on the configuration $1^4 3^2 2^1$ then
there must also exist the (3/2⁻) base state of that series.

PREDICTED ROTATIONAL BANDS OF Li[7]

COMPARED TO

EXPERIMENTAL LEVELS
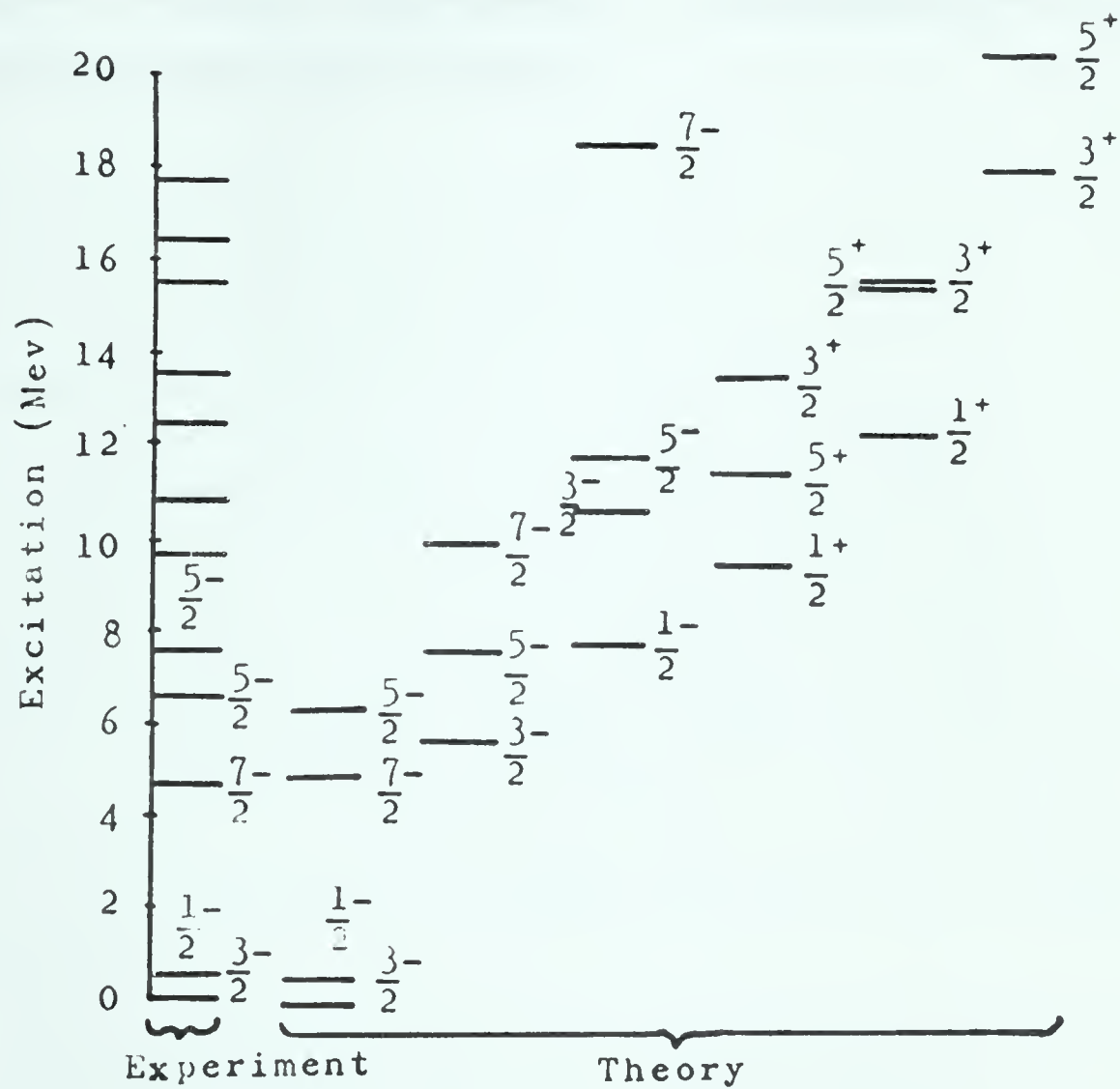
FIGURE II-2

The results of Chesterfield and Spicer predict the (3/2⁻) base state at 5.62 Mev. Such a state is not recognized in the compilation of Ajzenberg-Selove and Lauritsen (Aj59).

The overall agreement between experimental and theoretical levels as displayed in figure II-2 is surprisingly good. The most serious discrepancy is the prediction of the non-observed level at 5.62 Mev.

III STUDY OF Li^7 ENERGY LEVELS BY THE $Li^6(d,p)Li^7$ REACTION

1. Introduction

A (d,p) reaction is usually thought of as taking place by the stripping mechanism. However, in some cases, especially at low deuteron energies, this reaction may go via compound nucleus formation. In the former case the neutron is stripped off the bombarding deuteron and absorbed by the target nucleus. The proton whose neutron was stripped off continues in much the same direction of travel that it had just prior to the stripping, giving rise to the common forward distribution of protons. Theoretical predictions of stripping reaction angular distributions have been given by Butler (Bu51) and Bhatia et al (Bh52). In the case of compound nucleus formation the target nucleus and bombarding deuteron combine to form a highly excited compound nucleus which later emits a proton. In this case a more nearly isotropic distribution of protons is expected and observed.

In a stripping reaction the product nucleus is left at its ground state or at some excited level. The excess energy available for formation of the particular nuclear state shows up as kinetic energy and is split between the product nucleus and the emerging proton in such a way as to conserve momentum. This also applies in the case of compound nucleus formation.

Usually, for high Z target nuclei being bombarded by

high energy deuterons ($E_d > 20$ Mev), the attainable

energy levels in the product nuclei are closely spaced

and as a result proton spectra from such reactions will

appear continuous. On the other hand, the product

nuclei resulting from low energy deuteron bombardment

of low Z target nuclei display well spaced levels. In

that case there will be a group of protons correspond-

ing to every level in the product nucleus for which the

(d,p) cross-section is non zero at the particular

deuteron bombarding energy employed. The relative

number of protons in each group is proportional to the

cross-section for formation of the corresponding level

in the product nucleus. The angular distribution of

the individual groups will depend on the mechanism by

which the reaction takes place, for example, in the

case where Butler theory applies the angular momentum,

ℓ, of the absorbed neutron determines the angular

distribution.

If by some means proton spectra resulting from

deuteron bombardment of low Z target nuclei are obtained,

it is a straight forward but tedious task to deduce the

exact energy level of the product nucleus that the proton

groups belong to.

This section is devoted to a review of past work

on the $Li^6(d,p)Li^7$ reaction. The method employed to get the

proton spectra as well as the results obtained will be studied. The order of presentation is chronological.

2. The Work of Rumbaugh, Roberts and Hafstad

The work of Rumbaugh, Roberts and Hafstad on the $Li^6(d,p)Li^7$ reaction (Ru38) was mainly concerned with the deuteron energy dependence of the yield. The results of their experiments are of not much interest here. However, their experimental approach will be outlined for the sake of completeness.

The target used was 18 micro gram per square centimeter of Li^6, deposited on a copper backing in a mass spectrometer and subsequently oxidized in air. The deuterons were accelerated by an electrostatic generator having a stable energy range from 200 kev to 1 Mev.

Proton spectra were obtained in terms of their range in air. This was then converted to energy using the best range-energy curves available at the time. The actual detecting of the protons was done by an ionization chamber. The circuitry from the ionization chamber to the pulse counter was biased in such a way as to only count heavy ionizing particles near the ends of their ranges. To obtain the spectra runs were taken with various thicknesses of mica placed between the target and ionization chamber. The mica thicknesses had previously been calibrated in terms of the equivalent air ranges.

The proton groups corresponding to the ground and first excited state were observed. The energy of the first excited state of Li^7 as determined in their paper is 455 ± 15 kev. The error in this result is probably due to the poorness of the range-energy curves used.

3. The Work of Buechner, Straight, Stergiopoulos, and Sperduto

The work of Buechner et al (Bu48) on the $Li^6(d,p)Li^7$ reaction consisted of a more accurate determination of the first excited level in Li^7. As in the experiment of Rumbaugh et al the deuteron beam was obtained from an electrostatic accelerator and the target used was Li^6 deposited on a thin backing by a spectrometer. They too limited themselves to observations of the proton spectra at 90° to the incident beam.

The main point of interest in their experiment is the means of obtaining the proton spectra. Use was made of a large annular magnet which produced a variable uniform field over an annular region having a mean diameter of 70 centimeters and an annular width of 5 centimeters. The pole faces were 14 mm apart. The target was contained in a chamber placed in a slot cut through the annular region. Diametrically opposite the target another slot was cut in which nuclear photographic plates were placed. A thin walled vacuum chamber was placed in the annular region between the pole faces so as to contain both the target and the photographic

plate. With this arrangement, for any arbitrary setting
of the magnetic field strength, a small part of the proton
spectrum at 90° focussed on the plate. The entire proton
spectrum at 90° is then obtained by taking successive
runs slowly incrementing the magnetic field strength. The
magnetic field strength was calibrated in terms of energy
by taking the spectra of various alpha sources. The
plates were read by use of a darkfield binocular microscope.

For a deuteron energy of 1.38 Mev the proton peaks due
to formation of the ground and first excited states of Li^7
were found to be separated by 422 kev. From this the energy
level of the first excited state of Li^7 was calculated to
be 483 ± 6 kev. No search was made for proton groups cor-
responding to higher levels in Li^7.

4. The Work of Gelinas and Hanna

Gelinas and Hanna (Ge52) were the first to report ob-
serving the proton group from the 4.6 Mev level in Li^7.

The target used in their experiment was prepared by
evaporating natural lithium (7.5% Li^6, 92.5% Li^7) onto a
1000 Å nickel foil. Runs were made at deuteron bombar-
ding energies of 0.91 and 1.03 Mev. Detection of the reac-
tion products was by means of nuclear plates in a magnetic
spectrograph. Individual spectra were obtained from single
three inch plates. The energy scale was determined from the
deuterons elastically scattered by Li^7. The reaction products

were observed at 90° and 110°. For these combinations of bombarding energy and observation angle of the emitted pro-tons, the Li^7 excited energy range from 4.30 to 4.80 Mev was covered.

A weak group of protons was observed whose shift in energy with angle and bombarding energy identified it as a proton group from the $Li^6(d,p)Li^7$ reaction. The excitation energy of Li^7 corresponding to the observed group was deter-mined to be 4.61 $\pm$ .02 Mev.

5. The Work of Holt and Marsham

The work of Holt and Marsham on the $Li^6(d,p)Li^7$ reac-tion (Ho53) was designed to give forward distributions of the proton groups corresponding to the ground and first excited states of Li^7. Their apparatus was designed to allow intensity measurements on proton groups of higher energy than the incident deuteron beam over the angular region from -5° to +140°.

In their experiment, 8 Mev deuterons from a cyclotron bombarded a target prepared by evaporation of a solution of the carbonate of Li^6 onto a thin gold foil. At the back of the target chamber there was a strip of gold just thick enough to stop the deuteron beam. Protons of suffi-cient energy would pass through the gold strip and out of the target chamber through a cellophane window.

The protons were detected by a triple proportional

counter after passing through a variable pressure air cell
and one of a number of available thicknesses of aluminum
foil. The triple proportional counter was made up of three
proportional counters lined up with the target, air cell,
and aluminum foil and with only single walls separating
adjacent counters. Pulses from the three counters were
fed into a coincidence unit which recorded only pulses from
the first two counters not accompanied by a pulse from the
third counter. This means that only particles that were
stopped in the wall between the second and third counter
were recorded. For a certain combination of pressure in the
variable pressure air cell and thickness of aluminum absor-
ber there was then a corresponding small range of proton
energies that would be recorded. The width of this energy
range depends on the thickness of the wall between the
second and third counter. So, by varying the air pressure
and thickness of the absorber it was possible to obtain
charged particle spectra. The coincidence unit was made
sensitive to the difference in pulse heights produced in the
first two counters and in this way it was able to distinguish
between protons and other charged particles.

The angular distributions at forward angles of less
than 60° were fitted to Butler theory by taking $\ell = 1$, and
the nuclear radius, r_o = 4.9 x 10^{-13} cm.

6. The Work of Levine, Bender, and McGruer.

The work of Levine, Bender, and McGruer on the $Li^6(d,p)Li^7$ reaction (Le55) gave much the same results as the work of Holt and Marsham. They too measured forward distributions of the proton groups corresponding to the ground and first excited states of Li^7.

The deuteron bombarding energy used in their experiments was 14.4 Mev. The targets used were prepared by evaporating natural lithium onto a thin silver foil right in the target chamber. The target chamber was constructed to allow charged particle analysis over a continuous range of 120°. Before detection the charged particles passed through a magnetic analyzer. The detector used was a CsI crystal cemented to a type 6292 Dumont photo-multiplier tube. Various aluminum foils could be rotated in front of the crystal to aid in identifying the particles by their pulse height and their energy loss in the foils.

Angular distributions were obtained for the proton groups corresponding to the ground and first excited states of Li^7. The best fit for angles below 50° to Butler theory was obtained by taking $\ell = 1$ and $r_o = 5.4 \times 10^{-13}$ cm. They also reported a level at 6.56 Mev in Li^6 for which no angular distribution was taken. This level was later reported to be due to a contaminant (Ha58).

7. The Work of C. P. Browne

Browne (Br57) reports on the results of 7.0 and 7.5 Mev deuteron bombardment of LiOH. The proton groups were recorded in nuclear track plates exposed in the MIT broad-range spectrograph. The high resolution of the spectrograph allowed a direct measurement of the widths of two of the levels in Li^7. Angles of observation were 30, 70, and 90 degrees.

The three excited Li^7 levels observed were 0.47, 4.6 and 7.5 Mev. The exact results for the latter two levels were: 4.630 Mev with a natural width of 93 $\pm$ 8 kev and 7.45 Mev with a width of 91 $\pm$ 8 kev. No level was observed at 5.5 Mev.

8. The Work of Hamburger and Cameron

Hamburger and Cameron (Ha58) report on the results of bombardment by 15 Mev deuterons of metallic Li^6 targets. The outgoing particles were magnetically analyzed and recorded in nuclear emulsion. Angular distributions from 10° to 90° were obtained for the 4.6 and 7.5 Mev levels. The 7.5 Mev level cross-section could at low angles be fitted to an $\ell = 1$ Butler curve; its reduced width for $r_o = 4.5 \times 10^{-13}$ cm was found to be approximately equal to that of the ground state. The angular distribution corresponding to the 4.6 Mev level was found to be nearly isotropic, the differential cross-section being roughly 1/16 of

the ground state cross-section at 15°.   Spectra were obtain-
ed at 11°, 15°, and 25°; no other narrow ($\Gamma < 120$ kev) levels
of comparable cross-section were observed between 0.5 and
14 Mev excitation.

In a later paper (Ha60) Hamburger and Cameron give a
more detailed discussion of their work. From the examina-
tion of spectra at 11°, 15°, 25° and 45° the following upper
limits on unobserved cross-sections in the Li^7 excitation
range from 4.6 to 7.5 Mev were estimated. Any level of
width $\Gamma \leq 200$ kev should have been observed if it has a
cross-section greater than 0.5 mb/sterad, and levels with
$\Gamma \leq 500$ kev should have been observed if they have a cross-
section greater than 3 mb/sterad.

9. The Work of G. O. André

Angular distribution of the proton groups correspond-
ing to the ground and first excited states of Li^7 for 1.57
Mev bombarding deuterons were obtained by G. O. André (An60).

The target used by André was 30 micro grams per square
centimeter of natural lithium in the form of Li$_2$O supported
on a 200 micro inch copper foil. The protons were recorded
in emulsions placed with their central points circularly
around the target. The emulsions were shielded from the
scattered deuterons by a one hundred micro inch nickel
foil supported on a cylindrical frame.

The absolute angular distributions in the centre of mass

system given in the original paper are reproduced here as figure III-1 and figure III-2.

To explain the shape of the angular distributions the total (d,p) cross-section was assumed to be due to a combination of both deuteron stripping and compound nucleus formation. The interference between stripping and compound nucleus formation was taken into account. The broken line represents the estimated contribution due to compound nucleus formation. The solid line is obtained as a result of calculations for an $\ell = 1$, $r_o = 6.7 \times 10^{-13}$ cm, Butler-Born approximation.

ANGULAR DISTRIBUTIONS OF PROTON GROUPS

FROM THE Li^6(d,p)Li^7 REACTION

AT E$_d$ = 1.57 MEV

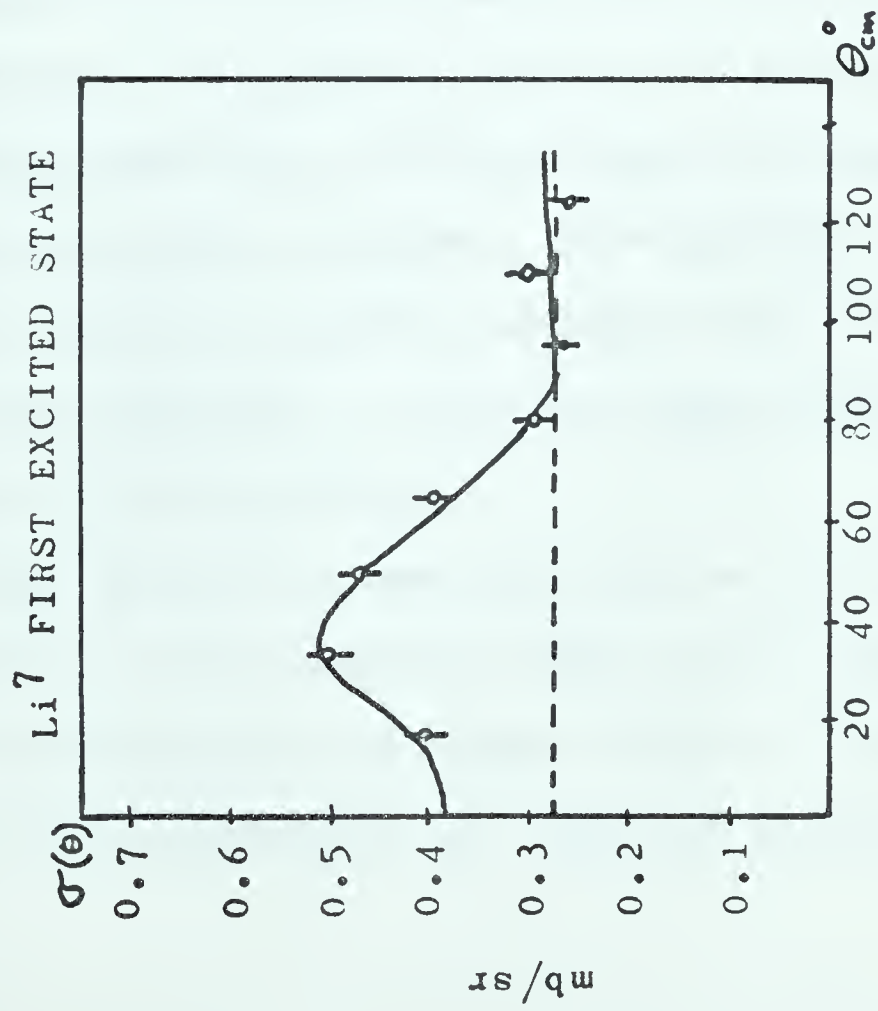
Li^7 GROUND STATE

FIGURE III-2

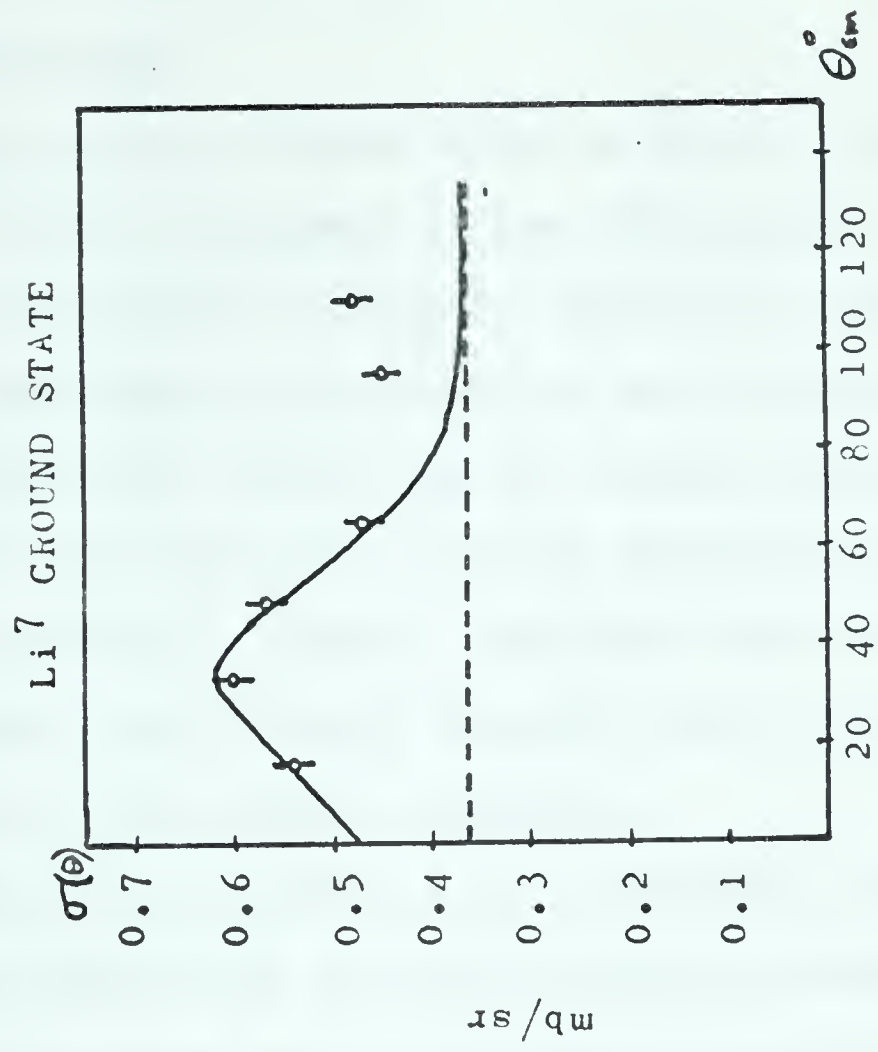Li^7 FIRST EXCITED STATE

FIGURE III-1

IV EXPERIMENTAL SEARCH FOR A NONOBSERVED 5.6 MEV LEVEL IN Li^7

1. Introduction

The previous chapter gives a fairly complete summary of work done in the past on the Li^6(d,p)Li^7 reaction. In all the experiments outlined, detection of the proton groups was based in principal on one or both of two basic energy dependent properties of charged particles: the radius of curvature in a uniform magnetic field and the range of flight in matter. Another thing that all these experiments had in common was that much time was consumed in getting even a single spectrum.

There is available at the University of Alberta Van de Graaff Laboratory a system whereby spectra of charged reaction products as well as their angular distributions can be quite readily obtained. This system makes use of a third property of charged particles. The property used is the constancy, independent of type or energy of the incident charged particle, of the amount of energy lost per ion pair produced in silicon. The diffused junction semi-conductor detector and the surface barrier detector make use of this property. A detailed description of the system was given by Davids (Da62).

It was decided to use this system in a search for the nonobserved 5.6 Mev excited level of Li^7 predicted by the work of Chesterfield and Spicer (Ch63). The search was carried out by observing the reaction products of the

$Li^6(d,p)Li^7$ reaction.

2. Beam Hardware

The deuteron beam is accelerated by the 2 Mev Van de Graaff generator. After acceleration the beam is passed through an analyzing magnet into the roughly 10 foot long drift tube at the end of which the target chamber is placed. A carbon trap in the drift tube is designed to reduce contamination of the target.

The size of the beam incident on the target is controlled by a set of horizontal and a set of vertical 0.010 inch thick, tantalum beam defining plates in the drift tube. These plates can be moved in and out by means of micrometer screws making it possible to give the beam any desired rectangular shape to an accuracy of .001" in either direction. A quartz viewer immediately following the beam defining plates allows observation of the shape and focus of the beam. The beam defining plates controlling the horizontal position serve another useful purpose. It is the error signals from these plates that are used in the corona stabilization of the accelerating voltage.

The target chamber is constructed with a sliding vacuum seal in the horizontal plane of the beam to which the solid state detector is attached. This allows movement of the detector from -139° to 120° with respect to the incident beam direction. The insulated target holder

can be raised, lowered, moved sideways, and rotated

without breaking the vacuum in the system.

In the present work all targets have thin backings,

making it necessary to use a Faraday cup inside the chamber

to collect the beam. The beam current is measured with the

aid of a model A309A Current Indicator and Integrator*. To

insure a correct reading the target and Faraday cup are kept

at +300 volts with respect to the target chamber preventing

the escape of secondary electrons.

3. Target Preparation

The targets used were prepared by evaporation under

vacuum of metallic Li^6 onto 5 micro inch nickel backings

and subsequent exposure to air to allow oxidation.

The reason for requiring a thin target is as follows.

The Q value of the $Li^6(d,p)Li^7$ reaction going to the Li^7

ground state is 5.03 Mev. Therefore, the Q value for the

reaction going to the proposed 5.6 Mev level of Li^7 is

-.57 Mev. A proton group corresponding to this proposed

level will therefore at all angles be of less energy than

the most energetic deuterons that are Coulomb scattered

by the nickel backing at the same angle. The most energetic

scattered deuterons observed at any backward angle are

those that are scattered from the surface layers of the

nickel backing. Deuterons that are scattered from the

interior of the nickel backing will have lost additional

* Elcor Inc., Falls Church, Virginia, U.S.A.

energy in traversing the nickel up to the point of scat-
tering and again in traversing the distance of nickel
between the point of scatter and the detector. The spread
in scattered deuteron energies observed at any backward
angle is thus an increasing function of the thickness of
the nickel backing. For a thick backed target the energy
of scattered deuterons will have a continuous range from
the maximum energy at the angle of observation down to
zero energy. The solid state detector used does not
differentiate between the different types of low energy
charged particles. Hence, such a broad range of scattered
deuterons would completely obliterate any possible proton
groups as the Coulomb scattering cross-section of nickel
is much larger than any charged particle reaction cross-
section. So, to minimize the scattered deuteron back-
ground in the reaction product energy range of interest,
it is necessary to use as thin a backing as possible.

The nickel foil used for backings* comes in one inch
squares and is backed by a thin copper foil to allow hand-
ling. The nickel side of the double foil was glued to a
sturdy 3/4" by 1-1/2" piece of brass so as to cover a 3/8"
diameter circular hole in its centre. The piece of brass
was designed to fit the holder in the target chamber.
Great care was taken not to introduce any ripples or stress
in the part of the foil covering the 3/8" hole in the
brass as almost invariably this would later cause the nickel

* Chromium Corp. of America, Waterbury, Connecticut, U.S.A.

foil to break. After the glue dried, the copper foil backing the nickel foil was etched off by emersion in a solution of trichloric acid (100 gm/liter) and NH_4OH (500 ml/liter). Subsequently the nickel surface was washed by emersion in distilled water. The thinnest nickel foils successfully used as backings were 5 micro inches thick. Use of 2 micro inch foils was attempted but they invariably broke during either the etching or washing process.

Metallic Li^6 was evaporated onto the target backings prepared in the above manner by use of a model VS-9 evaporator*. The main features of the evaporator were a metal table with an opening to a vacuum pump in the centre and a transparent bell jar which with a rubber ring made a vacuum seal on the table. Mounted on the table was a set of leads to which a voltage was supplied from a variable ac supply outside the vacuum system. The leads were constructed so that a tantalum boat holding the material to be evaporated could be clamped between them. A stand holding the target backings was mounted on the table inside the bell jar. A shield that could from outside be inserted between the boat and targets or swung out of the way was also mounted on the table.

A piece of lithium metal weighing about 10 milligrams was used in each evaporation run. To keep the lithium from oxidizing while the bell jar was being pumped down a

* Veeco Vacuum Corp., New Hyde Park, Long Island, N.Y.

small drop of benzene was put in the boat along with the
piece of lithium. As the pressure came down the benzene
readily evaporated and was pumped out of the system. The
system was pumped down to a pressure of below 10^{-5} mm of
mercury. With the target shielded from the boat, a volt-
age was applied across the boat which just caused the
lithium to melt. The shield was then swung out of the
way of the targets for a number of seconds and then swung
back. The time of exposure depends on the thickness of
lithium desired on the targets. Three targets, each of
different lithium thickness, were prepared in a single
evaporation run by placing the three backings on the
stand at varying distances from the boat. The targets
were allowed to oxidize by slowly bleeding air into the
system.

4. Charged Particle Detection System

The detection system used by Davids (Da62) made use
of a diffused junction semiconductor detector. In the
present work use is made of a surface barrier detector.
The latter is made by thorough cleansing and polishing of
the surface of a slab of n-type silicon. A p-type layer
forms spontaneously on the surface. Electrical connection
is made by evaporating a thin gold film onto the surface.

The principal of operation of these two types of
solid state detector is the same. Electrons from the n-region

tend to diffuse to the p-layer and holes from the p-layer
tend to diffuse to the n-region. This results in the
erection of a potential barrier at the junction of the two
regions. This concentration of charges at the junction
leaves a charge carrier free space in both the p-layer and
n-region. An electric field exists in this charge carrier
free region. The charge carrier free thickness of the
silicon region is called the depletion depth. Any charges
injected into this depletion region are immediately col-
lected by the electric field giving rise to a voltage pulse
across the p-n junction. A charged particle passing through
silicon loses energy by creating ion pairs at the rate of
3.23 ev per hole-electron pair created. Therefore, if an
incident charged particle loses all its energy in the
depletion region, a voltage pulse proportional in height
to the energy of the particle will be observed across the
junction. The depletion depth may be increased by appli-
cation of a reverse bias to the detector. The depletion
depth varies roughly as the square root of the applied
voltage. The depletion depth also varies directly as the
square root of the resistivity of the silicon used. This
dependence of the depletion depth on bias voltage and
silicon resistivity allows design of detectors for various
charged particle energy ranges.

The detector used was a surface barrier type, model
PH 1-20-5*. A bias of -70 volts was employed. The signal

* Nuclear Diodes, Inc., Highland Park, Illinois.

pulses were amplified by an Ortec model 101 Preamplifier
and model 201 Amplifier*. Amplified pulses were fed into
the high voltage input of a model CN-110 256 channel pulse
height analyzer**.

5. Results

a) Means of Identifying Reactions

The results of this experiment are a number of
charged particle spectra. Peaks in these spectra corres-
pond to groups of particles emitted as the result of forma-
tion of product nuclei in discrete energy states. Peaks due
to elastic scattering of the incident beam are a special case
of this, with the product nucleus being the target nucleus
in the ground state. For a particular reaction initiated by
a deuteron beam of fixed energy, the energy of the observed
light reaction product varies with angle. This variation
of energy with angle allows positive identification of the
reaction in question.

In general, the relationship between the energy and
angle of observation of the light reaction product is cal-
culated in the following manner. The motion of the incident
deuteron and target nucleus is studied in the centre of mass
system. The sum of the initial kinetic energy in the centre
of mass system and the Q value of the reaction is the final
kinetic energy in the centre of mass system. The total

* Oak Ridge Technical Enterprises Corp., Oak Ridge, Tenn. U.S.A.
** Technical Measurement Corp., North Haven, Conn. U.S.A.

momentum in the centre of mass system is always zero.
Immediately following the reaction there are four unknown
variables of interest: the energy of the heavy reaction
product in the centre of mass system and its angle of
emergence, φ_{cofm}, with respect to the direction of the
incident deuteron beam, and the energy of the light reac-
tion product and its angle of emergence, θ_{cofm}. The above
conditions of energy and momentum conservation give three
relationships between these four variables. Hence, arbitra-
rily picking one of them fixes the other three. The centre
of mass variables are converted to the corresponding lab
variables by addition of the velocity of the centre of mass
to the velocity components in the incident deuteron beam
direction of the two product particles in the centre of mass
system. The outlined calculations are very tedious. There-
fore the problem has been programmed for a model 1620 IBM
Computer. The input data for this program are the masses
of the target nucleus, bombarding particle, product nucleus,
and the light reaction product, the Q value of the reaction
to the energy level of the product nucleus of interest, and
the energy of the bombarding particle. The output is in
tabular form. The observation angle of the light reaction
product, θ_{lab}, is listed in 5° intervals from 0° to 180°.
For every θ_{lab} the following information is given: θ_{cofm},
φ_{lab}, the kinetic energy of the light reaction product, the
kinetic energy of the product nucleus and the ratio of the

- 39 -

differential cross-section in the centre of mass system to
that in the lab system. The kinematics at the deuteron
energies to be employed for the reactions expected in the
bombardment of the oxide of Li^6 were run on the computer to
allow identification of the charged particle groups as they
were observed. The kinematics for reactions with C^{12} were
also run off as this is a common target impurity.

The variation with angle of the groups of scattered
deuterons from the various target nuclei can also be obtained
by use of the computer program. However, this was not done.
Instead, available graphs (Ma60) which give the ratio of the
scattered deuteron energy to the incident deuteron energy
as a function of observation angle and mass of the scatter-
ing nucleus were used.

b) General Features of the Spectra Obtained

As stated before, a selection of targets of various
thicknesses was prepared. After runs were made on the first
few targets it became apparent that every target used was
badly contaminated with carbon. The intensity of the carbon
peaks did not change much from the beginning to the end of
a set of runs on a particular target, indicating that the
carbon present was not due to deposition during the run but
rather that it was there before the run was started. To
further identify the origin of the carbon, runs were made on
a nickel target backing onto which no Li^6 had been evaporated.

The carbon peaks were evident there too. The most likely
source of the carbon appears to be the glue used to join
the nickel target backing to the brass holder. Time did not
permit experimenting to try producing carbon free targets.
It was decided to use that target which had the highest lithium
to carbon ratio as determined from the spectra while being
sufficiently thin to allow reasonable resolution of the peaks.

Spectra from the target decided on are given in figures
IV-1 to IV-13. All of these spectra were taken with the normal
to the target surface at 135° to the incident deuteron beam.
This geometry, of course, increases the effective target
thickness by a factor of $\sqrt{2}$. The deuteron energy employed
was 1.90 Mev. Spectra were taken at 10° intervals from 70°
to 130° and also at 139° to the incident deuteron beam. At
every angle of observation the spectrum was taken twice. The
first time, the amplifier gain was such that the proton groups
from the $Li^6(d,p)Li^7$ reaction to the ground state and first
excited state of Li^7 would correspond to the top channels of
the 256 channel pulse height analyzer. The second time the
spectrum was taken, the gain was increased so that the deute-
rons elastically scattered by the nickel backing corresponded
to the top channels. In the second run the integrated beam
current was five times that in the first run in order to give
better statistical results, as it was in the second spectrum
that it was hoped a proton group from a $Li^6(d,p)Li^7$ reaction
to the nonobserved 5.6 Mev level of Li^7 would be found.

The most prominent feature of every spectrum taken is the peak due to deuterons elastically scattered by the nickel target backing. The magnitude of this peak relative to that of other peaks is displayed in the spectrum of figure IV-1. As this peak is of little interest in this experiment it is left out in plots of the other spectra.

In the energy region below the nickel scattered deuteron peak there are three fairly prominent peaks. These are due to elastically scattered deuterons from O^{16}, C^{12}, and Li^6 respectively. The high gain spectra show that each of these peaks has a second peak of slightly lower energy associated with it. The magnitudes of these associated lower energy peaks are roughly half that of the main peaks in the case of the O^{16} and Li^6 scatter peaks and more nearly the same in the case of the C^{12} scatter peak. By use of the differential energy loss curves of Whaling (Wh57) it is found that the difference in energy between two associated peaks is equal to the energy lost by a deuteron in travelling through a thick- ness of nickel equal to that travelled in going from the front of the target to the back of it and from there through the thickness of nickel between the back of the target and the detector. From this it is concluded that these three associated peaks are also due to elastic scattering from O^{16}, C^{12}, and Li^6, except that in this case the scatterer is on the back face of the target backing rather than on the front of it. It is unfortunate that Li^6 (and therefore O^{16}) managed to get on the

LOW GAIN CHARGED PARTICLE SPECTRUM FROM Li^6 + d

E_d = 1.90 MEV

$THETA_{lab}$ = 100°

$Ni(d,d)$

'09

$O^{16}(d,p)O^{17*}$
(.871 Mev)

$O^{16}(d,p)O^{17}$

$O^{16}(d,\alpha)N^{14}$

$C^{12}(d,p)C^{13}$

$Li^6(d,p)Li^{7*}$
(.48 Mev)

$Li^6(d,p)Li^7$

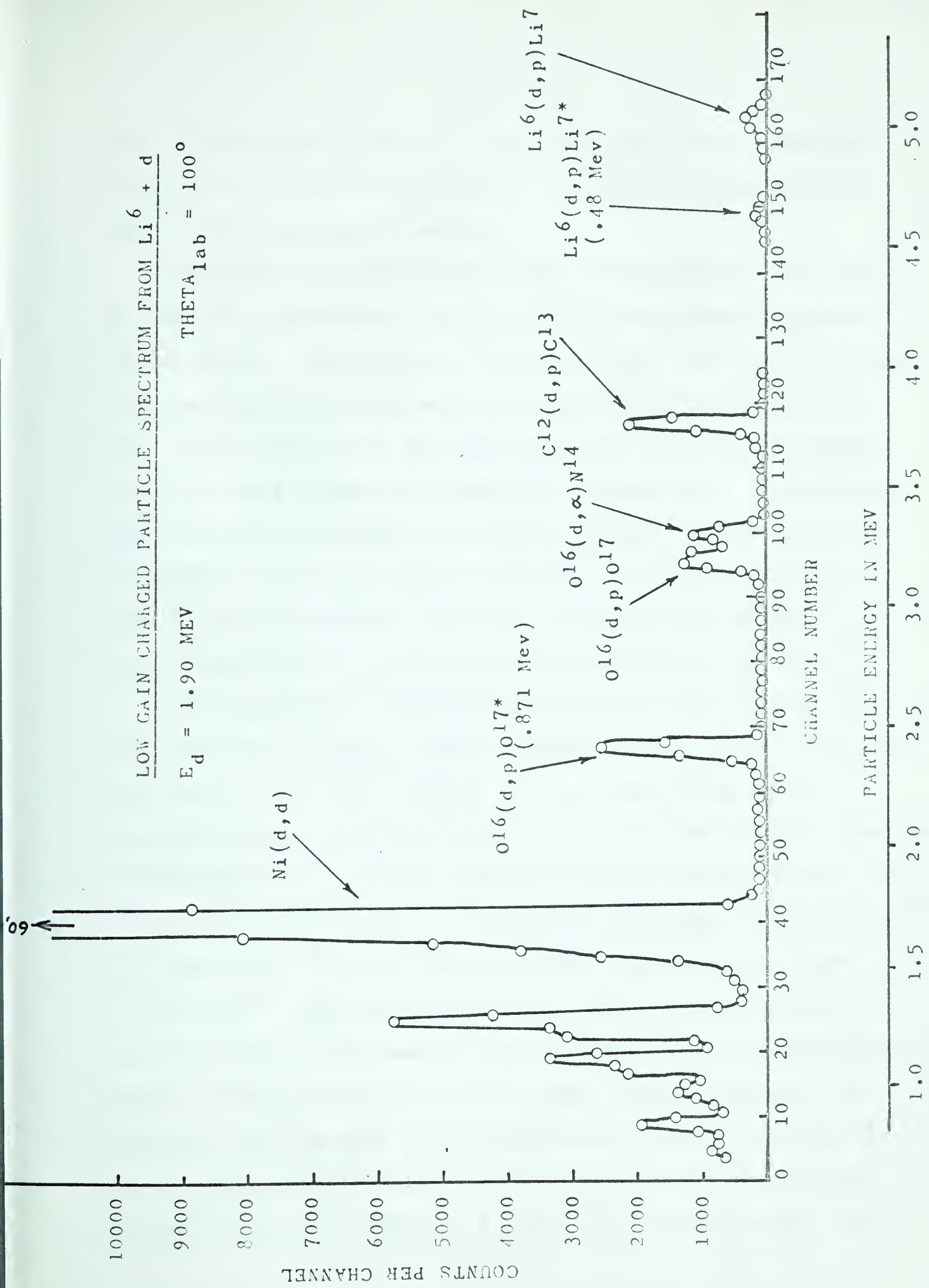COUNTS PER CHANNEL

CHANNEL NUMBER

PARTICLE ENERGY IN MEV

FIGURE IV-1

back of the target backing. This could have been prevented
by use of a shield on the side of the target remote from the
boat in the evaporation process.

One other prominent scatter peak is observed. This peak
is found by kinematics to be due to 0.95 Mev protons scatte-
red by nickel. The source of these protons are singly ionized
hydrogen molecules that are accelerated to an energy of 1.9
Mev. Since these have the same mass and charge as deuterons
they will pass through the analyzing magnet with the deuterons.
Upon entering the target the singly charged hydrogen molecule
is broken up into two .95 Mev protons. In some of the high
gain spectra very faint peaks are observed which energeti-
cally correspond to .95 Mev protons scattered by O^{16} and C^{12}.

The remainder of the prominent peaks in the spectra are
all identified as being due to either (d,p) or (d,α) reactions
with one of Li^6, C^{12}, or O^{16}. Six of these peaks appear
above the nickel scattered deuteron peak in the low gain spectra
of figures IV-10 to IV-13. These are due to proton groups from
$Li^6(d,p)Li^7$, $Li^6(d,p)Li^{7*}$ (.48 Mev), $O^{16}(d,p)O^{17}$, $O^{16}(d,p)O^{17*}$
(.87 Mev) and $C^{12}(d,p)C^{13}$ and an alpha particle group from
$O^{16}(d,\alpha)N^{14}$. The only one of these peaks that displays a
splitting due to the reaction taking place on two sides of the
target backing is the α-particle peak. This is because the
resolution at low gain is not sufficient to show the split in
proton groups but the alpha particle group split is resolved
because it is much larger as a result of the much higher rate

HIGH GAIN CHARGED PARTICLE SPECTRUM FROM Li^6 + d

E_d = 1.90 MEV

THETA$_{lab}$ = 70°

Prgton group locations for the Li^6(d,p) reaction to the imagined levels of Li7 indicated

Locations of known but not positively identified charged particle groups

5.40

5.50

5.60

5.70

O^{16}(d,α)

C^{12}(d,p)

O^{16}(d,p)

C^{12}(d,p)

COUNTS PER CHANNEL

CHANNEL NUMBER

PARTICLE ENERGY IN MEV
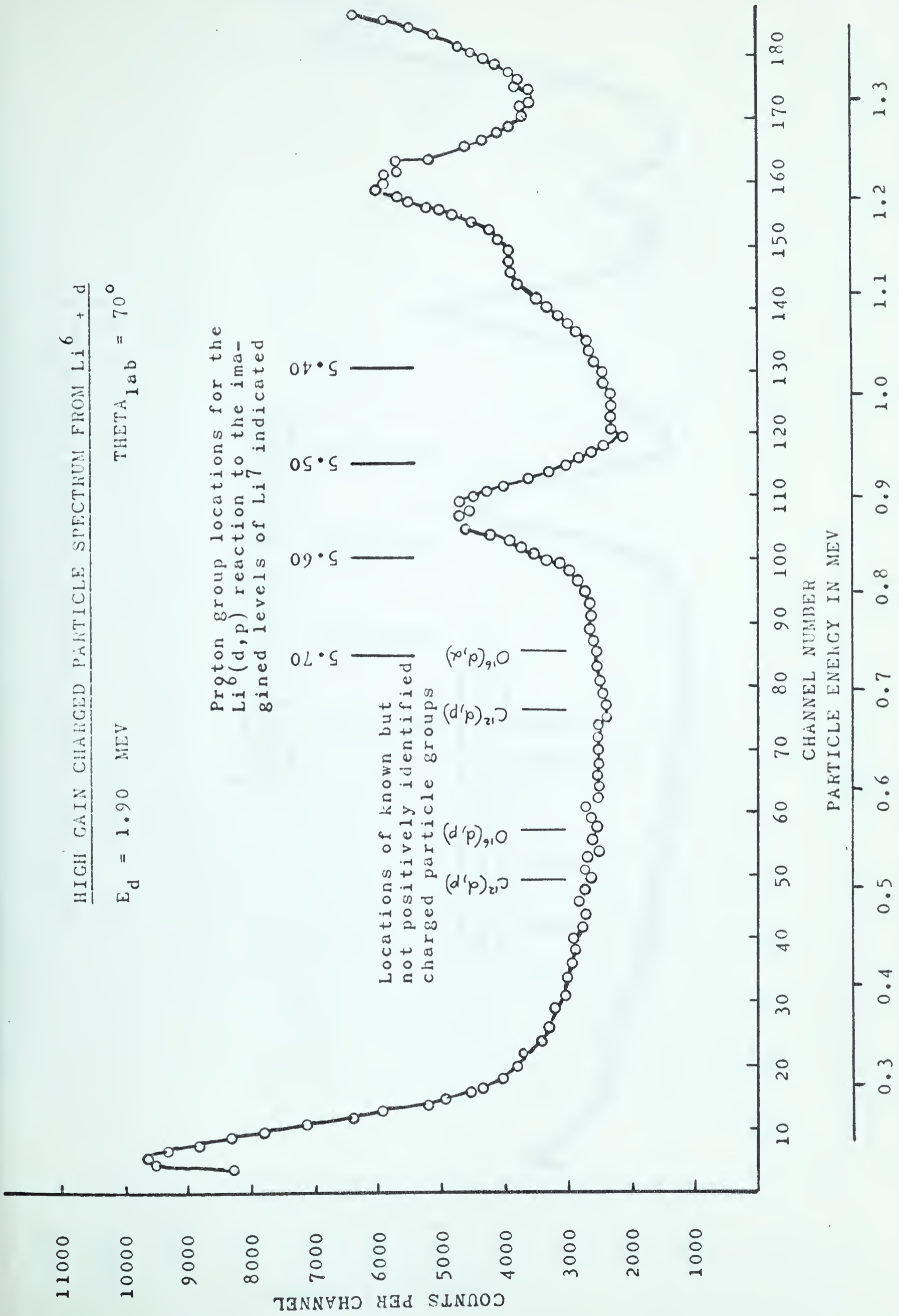
FIGURE IV-2

HIGH GAIN CHARGED PARTICLE SPECTRUM FROM Li^6 + d

$E_d = 1.90$ MEV

THETA$_{lab} = 80°$

Proton group locations for the Li^6(d,p) reaction to the imagined levels of Li^7 indicated

5.40

5.50

5.60

5.70

Locations of known but not positively identified charged particle groups

O^{16}(d,α)

C^{12}(d,p)

O^{16}(d,p)

C^{12}(d,p)

CHANNEL NUMBER

PARTICLE ENERGY IN MEV

COUNTS PER CHANNEL
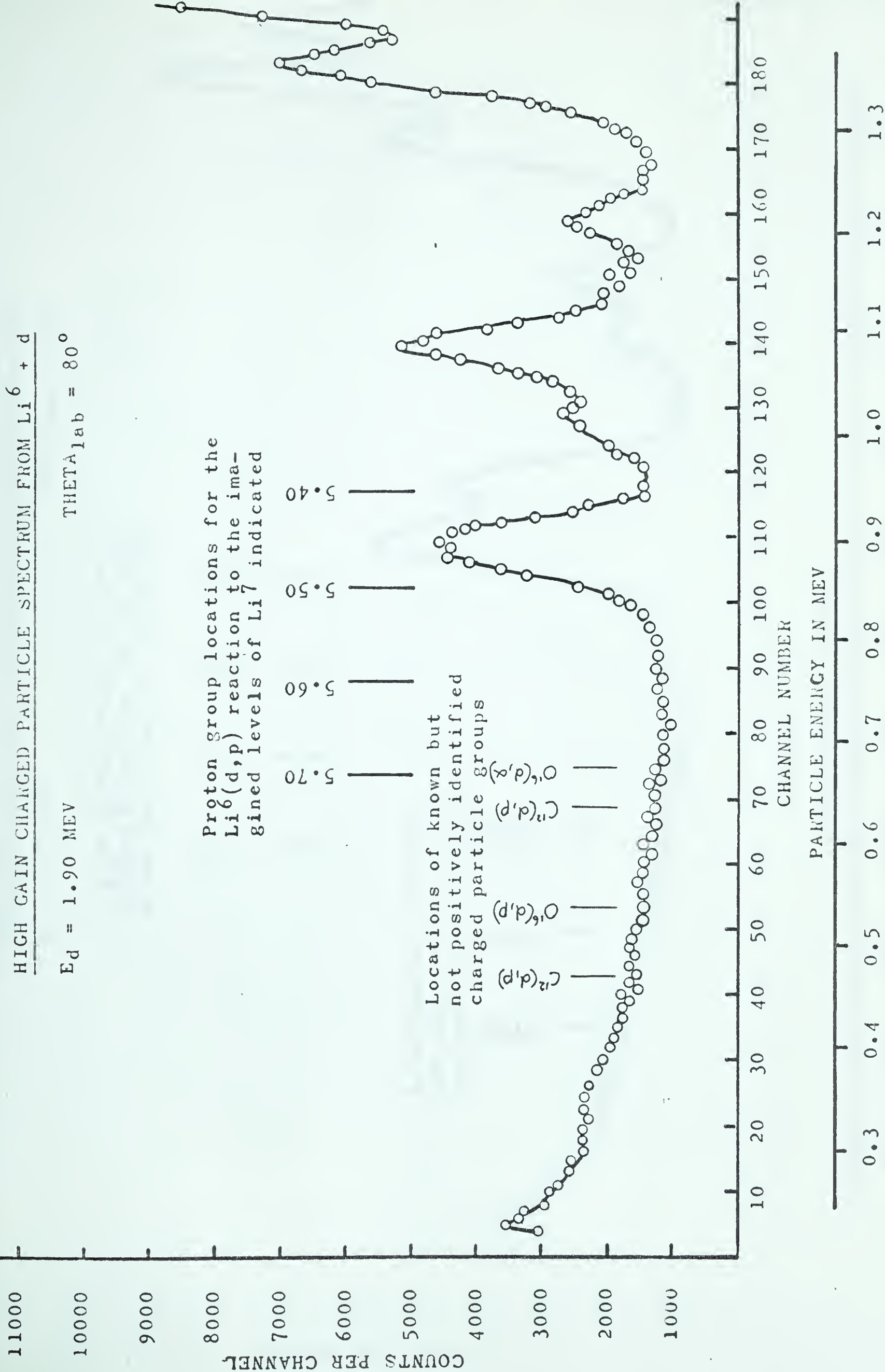
FIGURE IV-3

HIGH GAIN CHARGED PARTICLE SPECTRUM FROM Li⁶ + d

E_d = 1.90 MEV

THETA_lab = 90°

Proton group locations for the Li⁶(d,p) reaction to the imagined levels of Li⁷ indicated

5.40   5.50   5.60   5.70

Locations of known but not positively identified charged particle groups

C¹²(d,p)   O¹⁶(d,p)   C¹²(d,p)   O¹⁶(d,α)
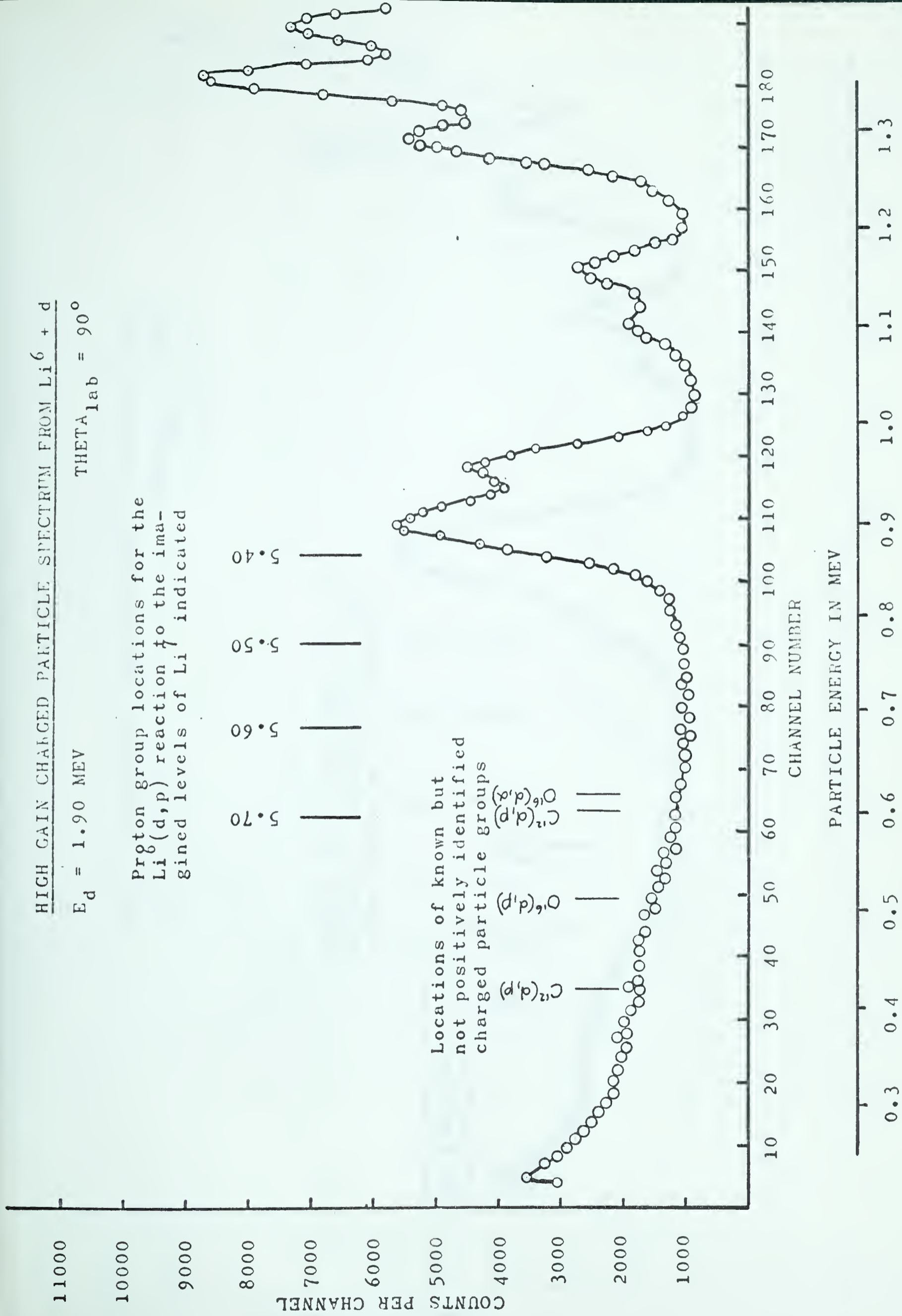
FIGURE IV-4

HIGH GAIN CHARGED PARTICLE SPECTRUM FROM Li⁶ + d

$E_d = 1.90$ MEV

$THETA_{lab} = 100°$

Proton group locations for the Li6(d,p) reaction to the imagined levels of Li7 indicated

5.40   5.50   5.60   5.70

O¹⁶(d,α)
C¹²(d,p)

O¹⁶(d,p)

C¹²(d,p)

Locations of known but not positively identified charged particle groups

COUNTS PER CHANNEL

CHANNEL NUMBER

PARTICLE ENERGY IN MEV

FIGURE IV-5

HIGH GAIN CHARGED PARTICLE SPECTRUM FROM Li^6 + d

E_d = 1.90 MEV

THETA$_{lab}$ = 110°

Proton group locations for the
Li^6(d,p) reaction to the ima-
gined levels of Li^7 indicated

Locations of known but
not positively identified
charged particle groups

5.40

5.50

5.60

C^{12}(d,p)
O^{16}(d,α)

5.70

O^{16}(d,p)

C^{12}(d,p)

CHANNEL NUMBER

PARTICLE ENERGY IN MEV

COUNTS PER CHANNEL

FIGURE IV-6

HIGH GAIN CHARGED PARTICLE SPECTRUM FROM Li^6 + d

$THETA_{lab}$ = 120°

E_d = 1.90 MEV

Proton group locations for the $Li^6(d,p)$ reaction to the imagined levels of Li^7 indicated

FIGURE IV-7

HIGH GAIN CHARGED PARTICLE SPECTRUM FROM Li^6 + d

E_d = 1.90 MEV

THETA$_{lab}$ = 130°

Proton group locations for the Li^6(d,p) reaction to the imagined levels of Li^7 indicated

Locations of known but not positively identified charged particle groups

C^{12}(d,p)

O^{16}(d,α)

O^{16}(d,p)

C^{12}(d,p)

COUNTS PER CHANNEL

CHANNEL NUMBER

PARTICLE ENERGY IN MEV

FIGURE IV-8

HIGH GAIN CHARGED PARTICLE SPECTRUM FROM Li⁶ + d

$E_d = 1.90$ MEV

$\text{THETA}_{lab} = 139°$

Proton group locations for the Li6(d,p) reaction to the imagined levels of Li7 indicated

5.40
5.50
5.60
5.70

Locations of known but not positively identified charged particle groups

$C^{12}(d,p)$
$O^{16}(d,\alpha)$
$O^{16}(d,p)$
$C^{12}(d,p)$

COUNTS PER CHANNEL

11000
10000
9000
8000
7000
6000
5000
4000
3000
2000
1000

CHANNEL NUMBER

10 20 30 40 50 60 70 80 90 100 110 120 130 140 150 160 170

PARTICLE ENERGY IN MEV

0.3 0.4 0.5 0.6 0.7 0.8 0.9 1.0 1.1 1.2 1.3
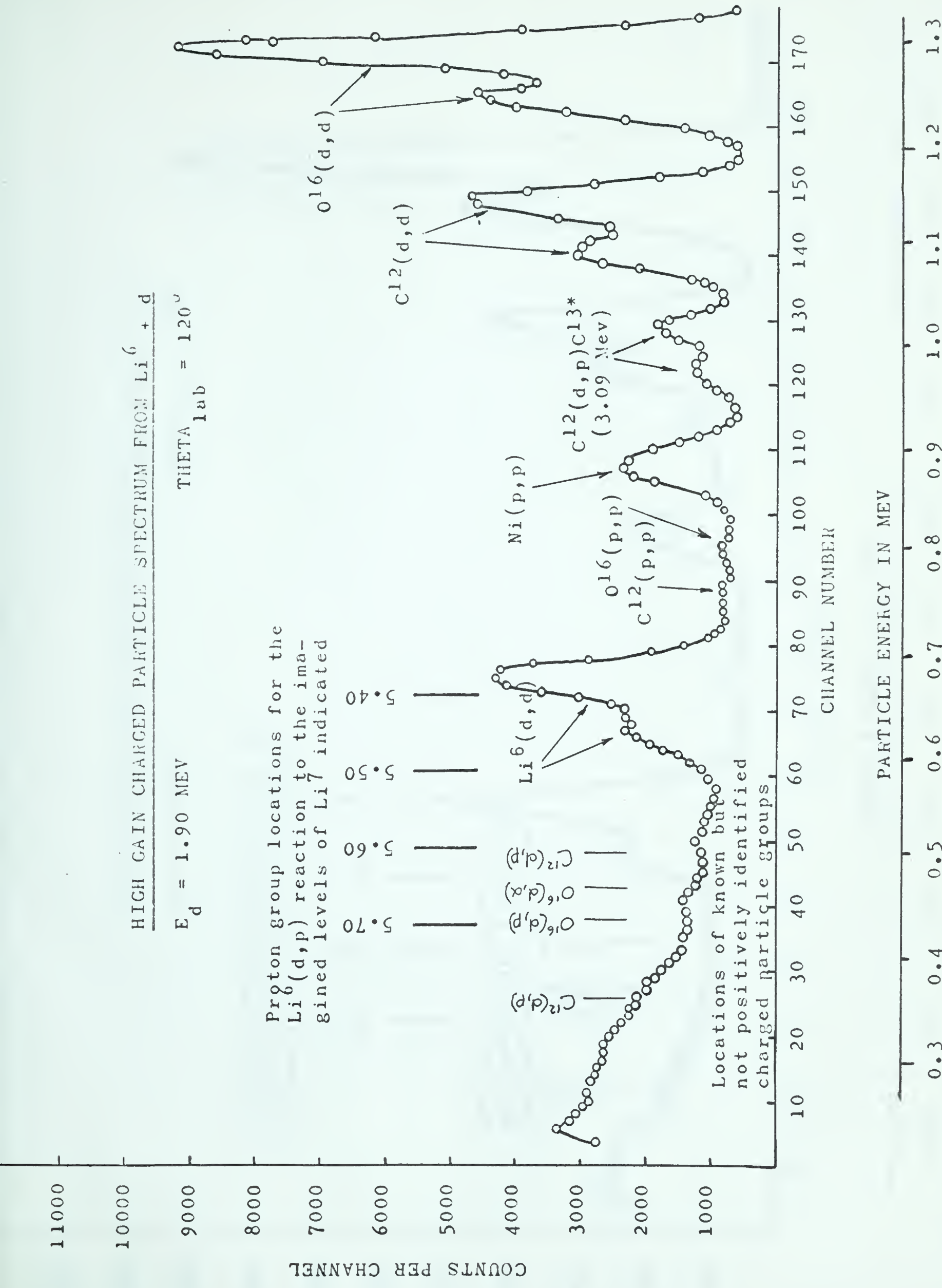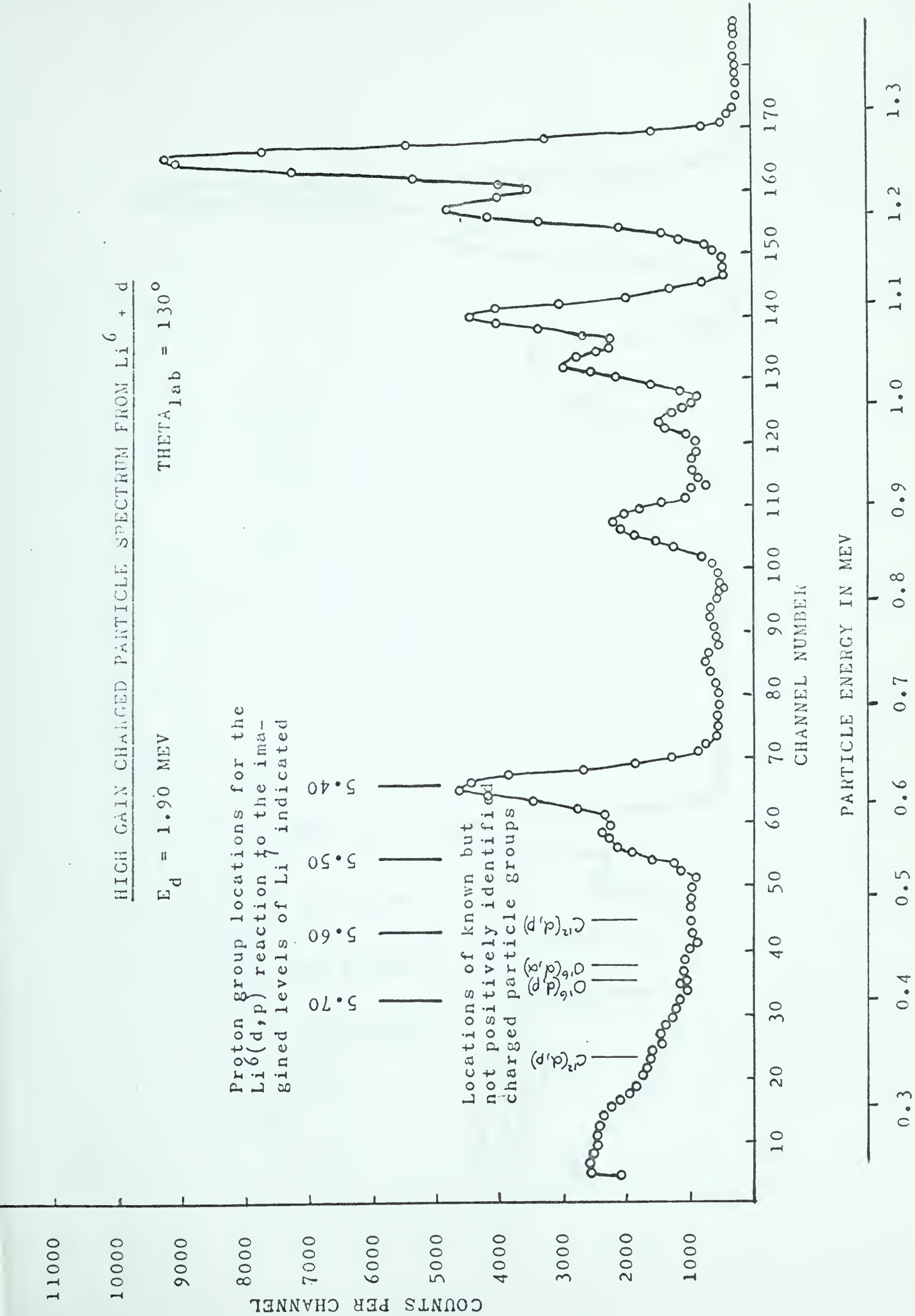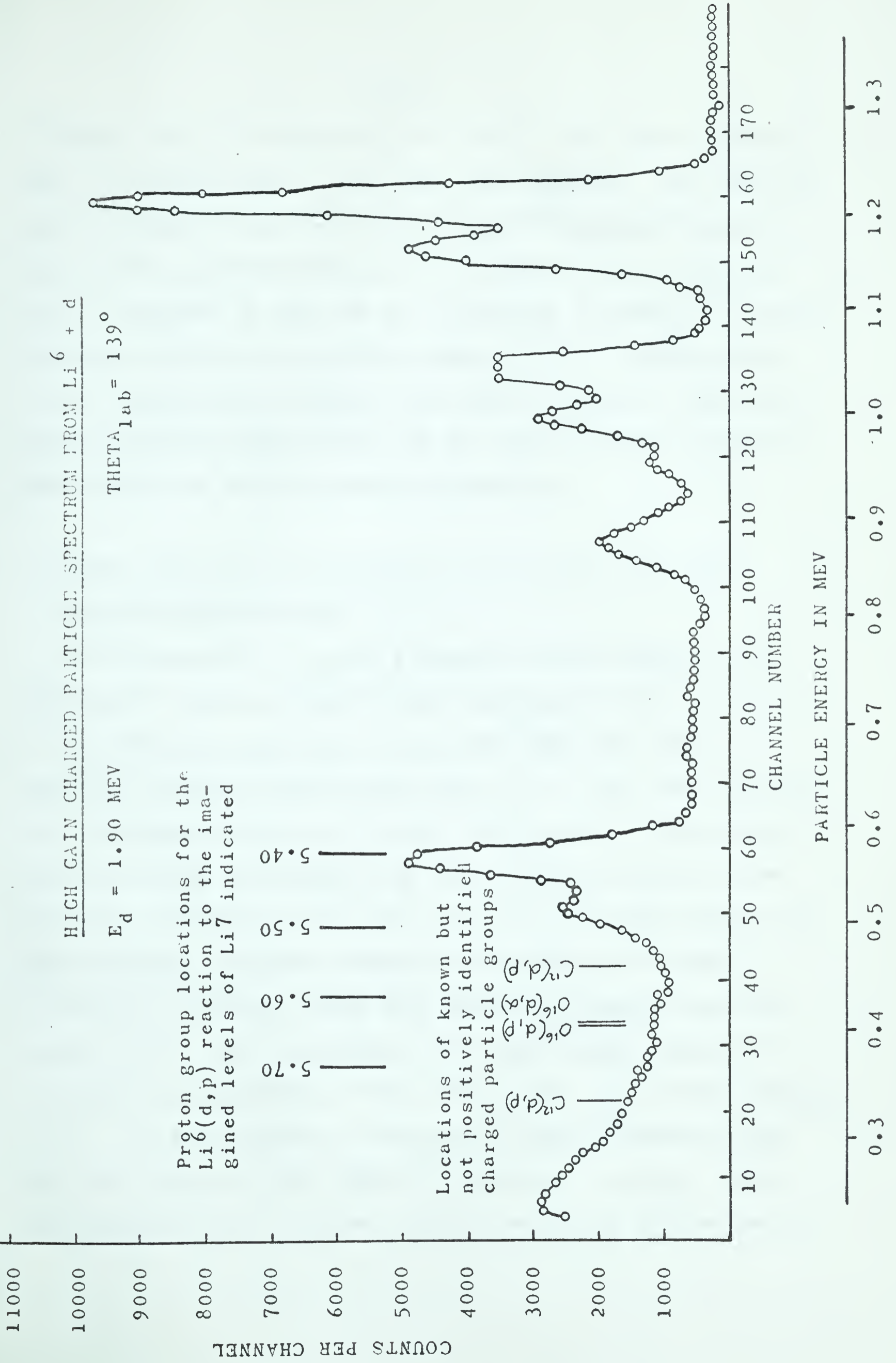
FIGURE IV-9

of energy loss of α-particles in nickel. One other prominent peak is found on some of the high gain spectra. This peak is due to a proton group from the $C^{12}(d,p)C^{13}$ reaction going to the 3.09 Mev excited state of C^{13}. A peak that is expected but not observed is the one due to protons from the $Li^6(d,p)Li^7$ reactions going to the 4.6 Mev level of Li^7. A good reason for not being able to observe this peak is that in the region where it should appear there are the various deuteron scatter peaks which are of much greater intensity.

c) Upper Limit on the Nonobserved $Li^6(d,p)Li^7$ (5.6 Mev) Reaction Cross-section

In an attempt to locate a possible proton group from a $Li^6(d,p)Li^7$ reaction going to the predicted 5.6 Mev level of Li^7 the following was done. The eight high gain spectra varying in angle of observation from 70° to 139° were plotted and are presented here as figures IV-2 to IV-9. The charged particle energy calibration was taken from the peaks due to deuterons scattered by Li^6, C^{12}, and O^{16}. On every graph the exact location of proton groups, corresponding to possible $Li^6(d,p)Li^7$ reactions going to a number of imagined excited levels of Li^7, were indicated. The proton group locations indicated corresponded to 5.40, 5.50, 5.60, and 5.70 Mev levels of Li^7. At some angles of observation there appeared to be very small peaks in the region of interest. However, these may have been due to charged particle reactions with either C^{12}
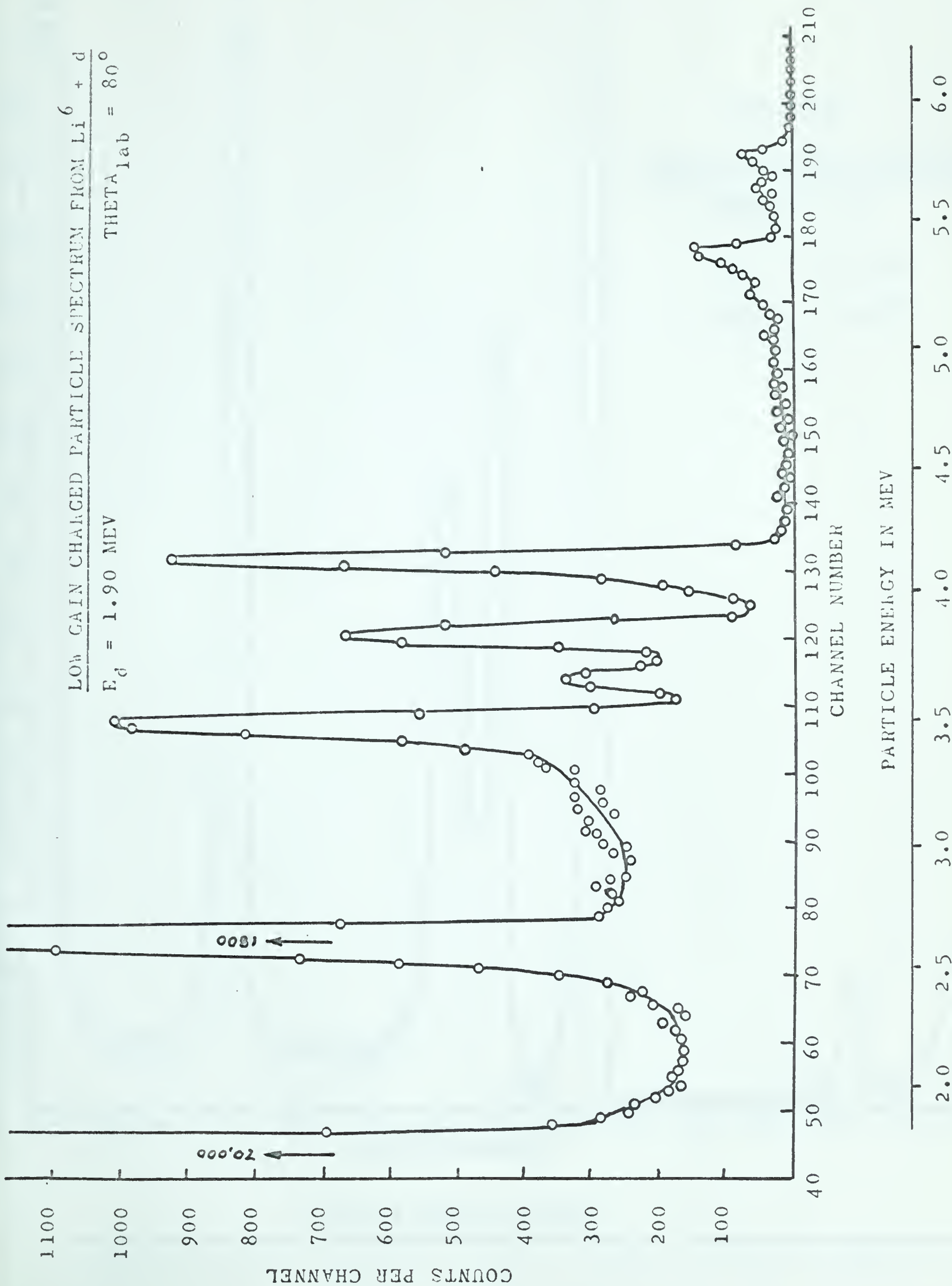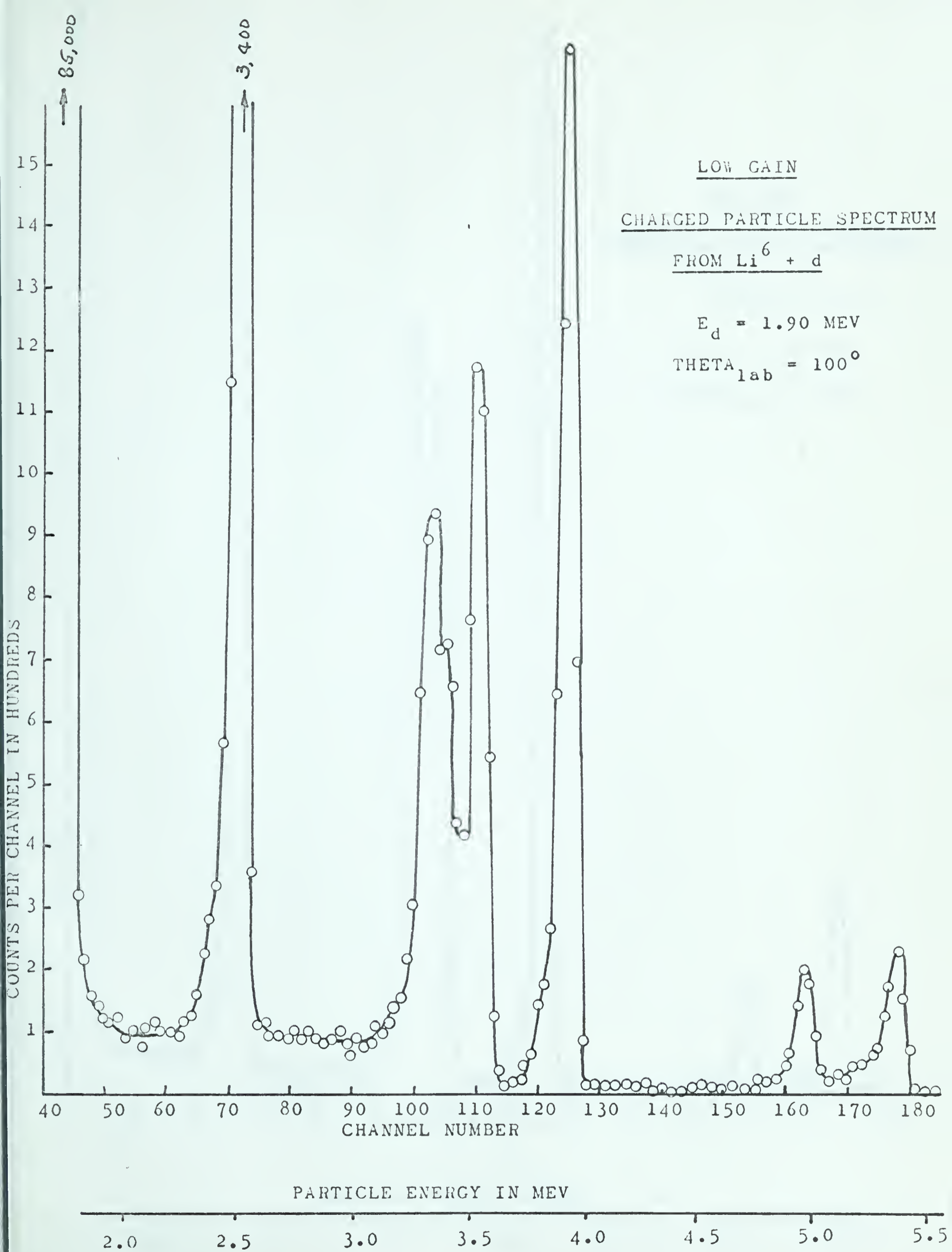
FIGURE IV-10

LOW GAIN CHARGED PARTICLE SPECTRUM FROM $Li^6 + d$

$THETA_{lab} = 80°$

$E_d = 1.90$ MEV

CHANNEL NUMBER

PARTICLE ENERGY IN MEV

COUNTS PER CHANNEL

FIGURE IV-11

LOW GAIN

CHARGED PARTICLE SPECTRUM

FROM $Li^6 + d$

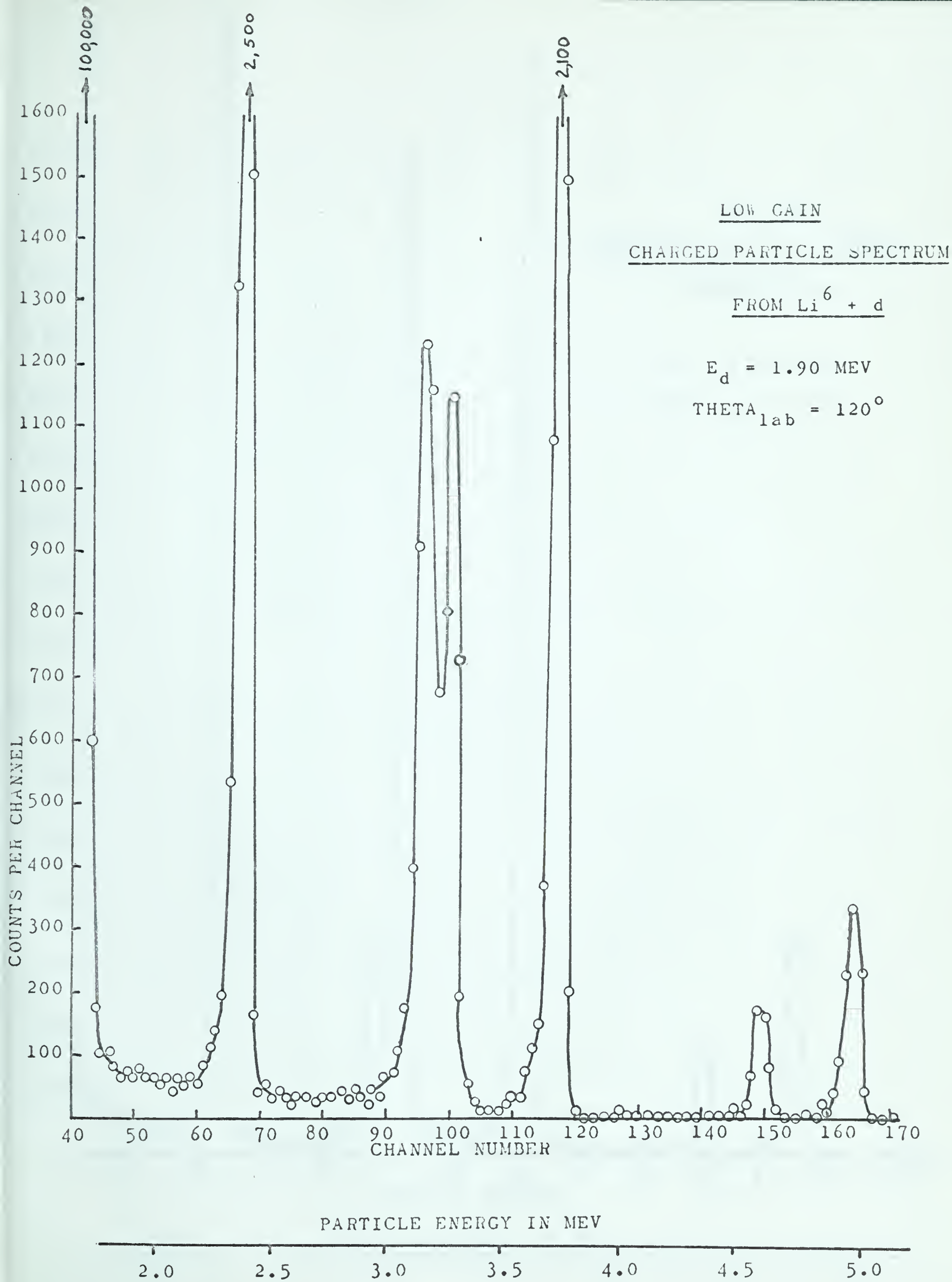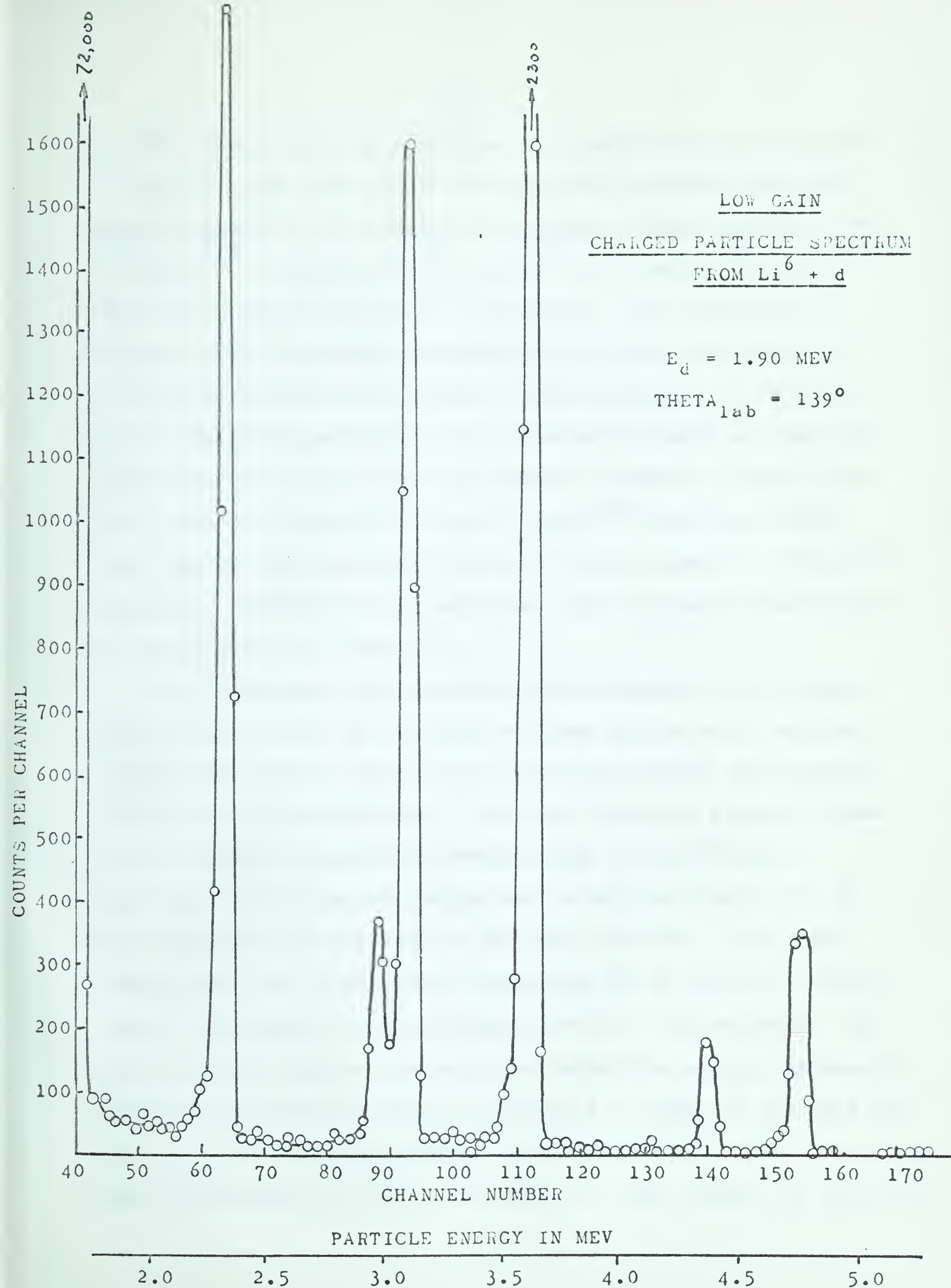$E_d = 1.90$ MEV

$THETA_{lab} = 120^\circ$

FIGURE IV-12

FIGURE IV-13

or O^{16}. There are four reactions that deuterons can have with C^{12} and O^{16} that will result in emission of charged particles having energies in the region of interest. These reactions are; $C^{12}(d,p)C^{13*}$ (3.68 Mev), $C^{12}(d,p)C^{13*}$ (3.86 Mev), $O^{16}(d,p)O^{17*}$ (3.06 Mev), and $O^{16}(d,\alpha)N^{14*}$ (3.95 Mev). The locations of charged particle groups corresponding to these four reactions are also indicated on the graphs of the spectra. It is diffi= cult to identify positively any of the small peaks as they are close together and not too well defined. However, they follow the locations predicted for the C^{12} and O^{16} reactions better than they do the locations predicted for any possible $Li^{6}(d,p)Li^{7}$ reaction. From this it is concluded that the peaks observed are in effect due to C^{12} and O^{16}.

It is estimated that positive identification of a proton group in the region of interest on these graphs would require a peak with a total number of at least 500 counts, spread over not more than four channels. The fact that such a peak follow= ing the angular dependence corresponding to a $Li^{6}(d,p)Li^{7}$ reaction is not observed can be used to set an upper limit on the differential cross-section for this reaction. The cross= section that 500 counts would correspond to is found by compari= son to the counts in the lithium scattered deuteron peak. For lack of better data at the deuteron bombarding energy employed the Rutherford scattering formula is assumed to apply at the most for= ward angle at which the lithium scattered deuteron peak can be coun= ted. The spectrum at 70° is not useful in this respect as here the

deuteron peak in question coincides with the .95 Mev protons

scattered from nickel. At 80° the total number of counts in

the deuteron peak is 54,100. The Rutherford cross-section

at 80° is 18.2 mb/sterad. The upper limit on the cross-

section for the reaction in question is therefore given by

$\dfrac{500}{54,100}$ x 18.2 = .17 mb/sterad.

A check on this upper limit is made by use of the yields

from the $Li^{6}(d,p)Li^{7}$ reaction going to the ground and first

excited state of Li^{7} and the absolute differential cross-

section given in figures III-1 and III-2. These absolute

cross-sections are for E_{d} = 1.57 Mev but they will be assumed

to apply here as a short run at E_{d} = 1.50 Mev showed the proton

yield in question to be comparable at 1.50 Mev and 1.90 Mev

bombarding energy. The differential cross-section from figures

III-1 and III-2 must be corrected to change them from the centre

of mass system to the lab system. However, at 90° the correc-

tion is only a few percent. An average of the results ob-

tained by use of the yields of the two peaks at 110° gives an

upper limit on the differential cross-section of .05 mb/sterad.

6. Conclusion

Two upper limits on the backward angle differential cross-section for the $Li^6(d,p)Li^7$ reaction going to any narrow level of Li^7 around 5.6 Mev excitation have been obtained for a deuteron bombarding energy of 1.90 Mev. Of these two upper limits the one that was obtained by comparison to the yields of the $Li^6(d,p)Li^7$ reaction to the ground state and first excited state of Li^7 must be considered the better value. Use of the Rutherford scattering cross-section for Li^6 at 80° is a questionable procedure since for the most light scattering nuclei the deviation from Rutherford's formula is quite appreciable at such a large scattering angle. An upper limit on the differential cross-section for the reaction in question at backward angles is therefore .05 mb/sterad.

From this low upper limit on the $Li^6(d,p)Li^7$ differential cross-section to the predicted level and the non-observation of the level by other workers studying different reactions involving Li^7 (Aj59), it is concluded the level probably does not exist. A further indication of the level's non-existence is provided by the study of Be^7, the mirror nucleus to Li^7. The low lying energy levels of these two nuclei are strictly analogous. Here again no level is observed that would correspond to a 5.6 Mev level in Li^7 (Go63).

REFERENCES

Aj59   F. Ajzenberg-Selove, T. Lauritsen, Nuclear Physics
        11, 31 (1959)

An60   G. O. André, Nuclear Physics 15, 464 (1960)

Bh52   A. B. Bhatia, K. Huang, R. Huby, H. C. Newns, Phil.
        Mag. 43, 485 (1952)

Br57   C. P. Browne, Bull. Amer. Phys. Soc. 2, 350 (1957)

Bu48   W. W. Buechner, E. N. Strait, C. G. Stergiopoulos,
        A. Sperduto, Phys. Rev. 74, 1569 (1948)

Bu51   S. T. Butler, Proc. Roy. Soc. (London) A208, 559 (1951)

Ch63   C. M. Chesterfield, B. M. Spicer, Nuclear Physics 41,
        675 (1963)

Da62   C. N. Davids, M.Sc. Thesis, University of Alberta, (1962)

Ge52   R. W. Gelinas, S. S. Hanna, Phys. Rev. 86, 253 (1952)

Go63   D. F. Goble, M.Sc. Thesis, University of Alberta, (1963)

Ha58   E. W. Hamburger, J. R. Cameron, Bull. Amer. Phys.
        Soc. 3, 381 (1958)

Ho53   J. R. Holt, T. N. Marsham, Proc. Phys. Soc. A66,1032 (1953)

Ke55   A. K. Kerman, in "Nuclear Reactions", edited by Endt and
        Demeur (North-Holland Publishing Co., Amsterdam) Chapter
        10 (1959)

Le55   S. H. Levine, R. S. Bender, J. N. McGruer, Phys. Rev. 97,
        1249 (1955)

Ma60   J. B. Marion, Ed., "Nuclear Data Tables", U. S. Atomic
        Energy Comm., part 3, 130 (1960)

Ni55   S. G. Nilsson, Klg. Danske Videnskab. Selskab, Mat.-fys.
           Medd. $\underline{29}$, No. 16 (1955)

Ru38   L. H. Rubaugh, R. B. Roberts, L. R. Hafstad, Phys. Rev.
           $\underline{54}$, 657 (1938)

Wh58   W. Whaling, Handbuch der Physik $\underline{34}$, 193 (1958)